Design of a Laboratory Hall Thruster with Magnetically Shielded Channel Walls, Phase III: Comparison of Theory with Experiment

Ioannis G. Mikellides,[*] Ira Katz,[†] Richard R. Hofer[‡] and Dan M. Goebel[§]

Jet Propulsion Laboratory, California Institute of Technology, Pasadena, CA, 91109

Abstract: A proof-of-principle effort to demonstrate a technique by which erosion of the acceleration channel in Hall thrusters of the magnetic-layer type can be eliminated has been completed. The first principles of the technique, now known as "magnetic shielding," were derived based on the findings of numerical simulations in 2-D axisymmetric geometry. The simulations, in turn, guided the modification of an existing 6-kW laboratory Hall thruster. This magnetically shielded (MS) thruster was then built and tested. Because neither theory nor experiment alone can validate fully the first principles of the technique, the objective of the 2-yr effort was twofold: (1) to demonstrate in the laboratory that the erosion rates can be reduced by >order of magnitude, and (2) to demonstrate that the near-wall plasma properties can be altered according to the theoretical predictions. This paper concludes the demonstration of magnetic shielding by reporting on a wide range of comparisons between results from numerical simulations and laboratory diagnostics. Collectively, we find that the comparisons validate the theory. Near the walls of the MS thruster, theory and experiment agree: (1) the plasma potential has been sustained at values near the discharge voltage, and (2) the electron temperature has been lowered by at least 2.5-3 times compared to the unshielded (US) thruster. Also, based on carbon deposition measurements, the erosion rates at the inner and outer walls of the MS thruster are found to be lower by at least 2300 and 1875 times, respectively. Erosion was so low along these walls that the rates were below the resolution of the profilometer. Using a sputtering yield model with an energy threshold of 25 V, the simulations predict a reduction of ~600 at the MS inner wall. At the outer wall ion energies are computed to be below 25 V, for which case we set the erosion to zero in the simulations. When a 50-V threshold is used the computed ion energies are below the threshold at both sides of the channel. Uncertainties, sensitivities and differences between theory and experiment are also discussed.

E rosion of the acceleration channel in Hall thrusters can expose its magnetic circuit components to bombardment by beam ions, which can lead to the failure of the engine. This was recognized as a potential limitation of Hall thrusters for space missions early in their history. Although propulsive performance dominated their development at the beginning, techniques to reduce or eliminate channel erosion were considered as early as the 1960s. In an extensive review of stationary plasma thrusters (SPT) published in 2000, Morozov and Savelyev state: "…*at the beginning of the 1960s magnetic-force-line equipotentialization became known, and the chosen geometry of force lines (convex toward the anode) provided repulsion of ions from the walls by the electric field, thus reducing the channel erosion.*"[1] (For some of the first papers by Morozov *et al*. on line equipotentialization, see also Refs. 2 & 3.) Indeed, the advanced magnetic field topologies that are being used in many state-of-the-art (SOA) Hall thrusters today have led to improvements both in performance and wear.[4,5,6,7,8] However, channel erosion was never understood well enough to eliminate it or reduce it adequately to retire the risk for deep-space

---

[*] Member of the Technical Staff, Electric Propulsion Group, 4800 Oak Grove Drive, Pasadena, CA, 91109, Mail Stop 125-109, Associate Fellow AIAA.
[†] Group Supervisor, Electric Propulsion Group, 4800 Oak Grove Drive, Pasadena, CA, 91109, Mail Stop 125-109, Senior Member AIAA.
[‡] Member of the Technical Staff, Electric Propulsion Group, 4800 Oak Grove Drive, Pasadena, CA, 91109, Mail Stop 125-109, Senior Member AIAA.
[§] Section Staff, Thermal and Propulsion Engineering Section, 4800 Oak Grove Drive, Pasadena, CA, 91109, Mail Stop 125-109, Associate Fellow AIAA.

science missions. It has been largely due to this risk that Hall thrusters have never flown on NASA spacecraft despite their enabling propulsive capabilities.

Recently a new technique was proposed to eliminate channel erosion, based on findings from physics-based numerical simulations[9] with a magnetic-field-aligned-mesh (MFAM) code called *Hall2De*.[10] Termed "magnetic shielding," the technique recognizes the significance of deviations from "magnetic-force-line equipotentialization," which occur naturally in these devices due to the variation of the electron number density along the lines of force when the electron temperature is finite. Such deviations increase with higher electron temperature, and can occur not only inside the sheath that forms within a very thin layer near the channel walls, but also in the pre-sheath and in the plasma. The implication is that a component of the induced electric field along the magnetic field can (and usually is) established that accelerates some beam ions towards the walls causing erosion. As a result of this breakdown in the orthogonality of the two fields, a geometry of magnetic field lines with convex curvature toward the anode[1] cannot effectively control the electric field near surfaces (and, in turn, the erosion) if the near-wall lines are not also equipotential. Morozov had proposed that such equipotentialization may be achieved either by virtue of the internal conductivity of the channel or through the use of special annular electrode holders.3 Though unconventional electrode arrangements can indeed alter the relevant plasma properties[11] favorably, no arrangement has demonstrated in laboratory wear (or life) tests sufficient control of the electric field to sustain ~zero erosion throughout the test(s).

Magnetic shielding seeks to achieve ideal equipotentialization of the lines of force near the walls only and without the use special electrode arrangements. By doing so the near-wall plasma potential can be sustained, in principle, at values that equal (or are near) the discharge voltage without loss in thruster performance. In this manner the kinetic energy that ions gain through the potential drop in the plasma along surfaces can be eliminated or reduced significantly. We have argued that this can be achieved by taking advantage of the isothermal properties of the lines of force, with a magnetic field topology that extends lines adjacent to the walls deep into the anode region, where plasma electrons are cold (~1-3 eV).[10,12] Such magnetic field topology can be achieved without unusual or special electrode arrangements. In doing so, not only the contribution of the electron pressure to deviations from equipotentiality is marginalized but also the energy that ions gain through the sheath is reduced significantly. This ideal equipotentialization then allows for full control of the electric field by the magnetic field because it preserves their orthogonal properties. Magnetic shielding is distinctively different from other techniques currently being pursued to protect surfaces from erosion, like in the Highly Efficient Multistage Plasma Thruster (HEMP-T)[13] and the Diverging Cusped Field Thruster (DCFT).[14] These configurations exploit the magnetic mirror effect on electrons by employing multi-cusped magnetic fields to reduce plasma bombardment of the walls at the cusps. Such cusped arrangements provide also the magnetic field direction needed to induce the azimuthal electron motion and, in turn, the accelerating electric field at the cusped regions. In Hall thrusters with magnetically shielding there is no magnetic mirror effect because there are no cusps.

In 2009 a proof-of-principle effort began at the Jet Propulsion Laboratory (JPL) to demonstrate the first principles of magnetic shielding. Development of a new thruster was beyond the scope of this effort. Therefore, our approach was to modify the channel geometry and magnetic field of an existing thruster - a 6-kW laboratory Hall thruster called H6[15] - with the guidance of physics-based numerical simulation. Hereinafter we shall term this modified version of the thruster the "magnetically shielded (MS) configuration." The original or baseline thruster will be called the "unshielded (US) configuration." Numerical simulations and thruster modifications constituted Phase I of the design effort the results of which have been reported in the first of three papers on this subject.[12] Phase II comprised of an experimental effort that included wear diagnostics to compare the erosion characteristics of the two configurations. The results of this experimental campaign are reported in our companion paper.[16] It was recognized and emphasized early in the program that demonstration of reduced erosion rates in the laboratory, albeit necessary, cannot be sufficient without proof of the physics that led to such reductions. The experimental campaign therefore included also several plasma diagnostics to validate the theory. Phase III, the topic of this paper, brings together all our findings from the numerical simulations and the

experiments to conclude the demonstration of the magnetic shielding first principles. Section I summarizes the theoretical background (Sec. I.A), and is supported by results from our most recent simulations of the H6 thruster in both configurations (Sec. I.B). In Sec. II we report on a series of comparisons between the simulation results and measurements of the plasma and applied magnetic field (Sec. II.A), and of the erosion of the channel walls (Sec. II.B). The ultimate objective of all these comparisons is twofold: (1) to validate our understanding of the erosion physics in both configurations and (2) to demonstrate the capability to design a Hall thruster at a single operating point with orders of magnitude the life capability of its SOA counterparts. Ongoing efforts aim to demonstrate the effectiveness of magnetic shielding in high-power Hall thrusters, like the 20 kW-class NASA-300M designed, built and tested[17] at the NASA Glenn Research Center, and in lower-power thrusters like the H6 but at discharge voltages that exceed the nominal 300 V. We plan to report on the results of these efforts in future publications.

I.   Theory

A. Magnetic Shielding First Principles

The main objective of the proof-of-principle effort at JPL has been to demonstrate the first principles of magnetic shielding. These principles were discussed in detail in previous publications.[10,12] In this section we provide a summary of the main points for completeness. We begin with a brief review of well-known operational characteristics of Hall discharges as they are critical in establishing some of the key elements that allow magnetic shielding to be so effective. The number density of electrons (n_e) in Hall thrusters is low enough such that collisions in the azimuthal direction seldom impede their $\mathbf{E} \times \mathbf{B}$ drift, yielding in this direction a significant flow of current, the Hall current. The electric and magnetic fields are denoted by $\mathbf{E}$ and $\mathbf{B}$, respectively. Operation under these conditions implies a high value of the Hall parameter for the electrons, $\Omega_e \equiv \omega_{ce}/\nu_e \gg 1$, where ω_{ce} and ν_e are the electron cyclotron and total collision frequencies, respectively. As the Hall current crosses $\mathbf{B}$ the induced $\mathbf{E}$ is in the direction perpendicular ($\perp$) to $\mathbf{B}$ and proportional to $\sim \eta \Omega_e^2 \mathbf{j}_{e\perp}$ (according to Ohm's law). $\mathbf{E}_\perp/q_i$ serves as the main acceleration force on the ions. Here, the electron current density and resistivity are denoted by $\mathbf{j}_e$ and η, respectively. The increased resistive heating of the electrons in the region of high $\mathbf{E}$ leads also to an increase in the electron temperature (T_e). Typical profiles of the plasma potential (ϕ) and T_e along the channel centerline (CL) are shown in the schematic of **Fig. 1**-left.

Under these discharge conditions the resistance to the transport of heat and mass in the electron flow in a direction parallel ($\parallel$) to $\mathbf{B}$ is much smaller (by $\sim \Omega_e^2$) than that in the $\perp$ direction for most of the channel region. Thus, T_e remains relatively unchanged along the lines of force:

$$\nabla_\parallel T_e \approx 0 . \tag{I-1}$$

Moreover, in the absence of a resistive contribution to $\mathbf{E}$ in this direction the electron momentum equation simplifies to:

$$\mathbf{E}_\parallel \approx -T_e \nabla_\parallel \ell n(n_e) . \tag{I-2}$$

Equations (1) and (2) yield respectively two well-known properties of the lines of force in these thrusters2;3: $T_e \approx T_{e0}$ and $\phi \approx \phi_0 + T_{e0} \ell n(n_e/n_{e0})$ along a magnetic field line, where T_{e0}, ϕ_0 and n_{e0} denote integration constants. Thus, though each line is nearly isothermal it is not also of fixed potential unless the electron temperature is zero.3 This allows for a finite component of $\mathbf{E}$ parallel to $\mathbf{B}$ which, in turn, can lead to ion acceleration towards the containing walls if the $\mathbf{B}$-lines begin/terminate at the surface of the material. Erosion of the channel walls occurs when ions strike them with sufficient energy to sputter off material.

Deviations from equipotentiality along lines of force near the channel walls has been the main reason that most SOA Hall thruster designs have continued to exhibit channel erosion. It is worthwhile noting that this includes modern thrusters that have achieved significant improvements in performance by way of more advanced "plasma-lens" configurations (e.g. compared to the older SPT-like designs). To better

illustrate the main impediment we use as an example a typical SPT-like magnetic field configuration as depicted in Fig. 1-middle. We designate this as a "US configuration." Here the variation of ϕ and T_e along the walls is similar to that along the CL because the lines are nearly radial. Consequently, the elevated $E_\parallel$ and T_e at the walls can drive a flux of high-energy ions to the walls. The induced erosion can be reduced if the curvature of lines is made more convex towards the anode as originally proposed by Morozov et al. Other approaches have been proposed by way of atypical electrode arrangements.[3,11] But there has never been a Hall thruster design that has demonstrated in a laboratory wear test zero channel erosion (or reductions by orders of magnitude compared to the SOA) from the beginning until the end of the test.

Referring to Fig. 1-right, magnetic shielding is achieved by way of a magnetic field topology that sustains high ϕ and low T_e near the channel surfaces, in fact, as close as possible to the discharge voltage V_d and to the coldest values of T_e that can be attained inside the channel, respectively. In this manner the incident-ion kinetic and sheath energies can be marginalized. Moreover, with a properly designed combination of **B** and channel geometry, **E** can be controlled to be both nearly perpendicular to the surface and large in magnitude, as shown in the MS configuration Fig. 1-right. That is, magnetic shielding seeks to achieve ideal equipotentialization of the lines of force near the walls. In this manner the induced $E_\perp$ forces ion acceleration away from walls without loss of thruster performance. This also reduces the wall-incident ion flux. It is emphasized that a change in the geometry of the wall alone, e.g. chamfering of the surface, is not sufficient as it has been demonstrated in our tests.[16] This will be discussed further later. The key principle behind magnetic shielding lies in the recognition that the electron pressure (yielding $T_e \times \ln(n_e)$ in Eq. (I-2)) forces **E** and **B** to no longer form an orthogonal set (Fig. 1-middle). Thus, a geometry of **B**-lines with convex curvature toward the anode[1] cannot effectively control **E** near surfaces (and, in turn, the erosion) if the near-wall lines are not also equipotential. In contrast, Fig. 1-right shows a magnetically shielding **B** topology. This topology eliminates the contribution of the electron pressure by exploiting those **B**-lines that extend deep inside the acceleration channel, near the anode. Because these lines are associated with high ϕ_0 and low T_{e0} the contribution of $T_e \times \ln(n_e)$ is marginalized.
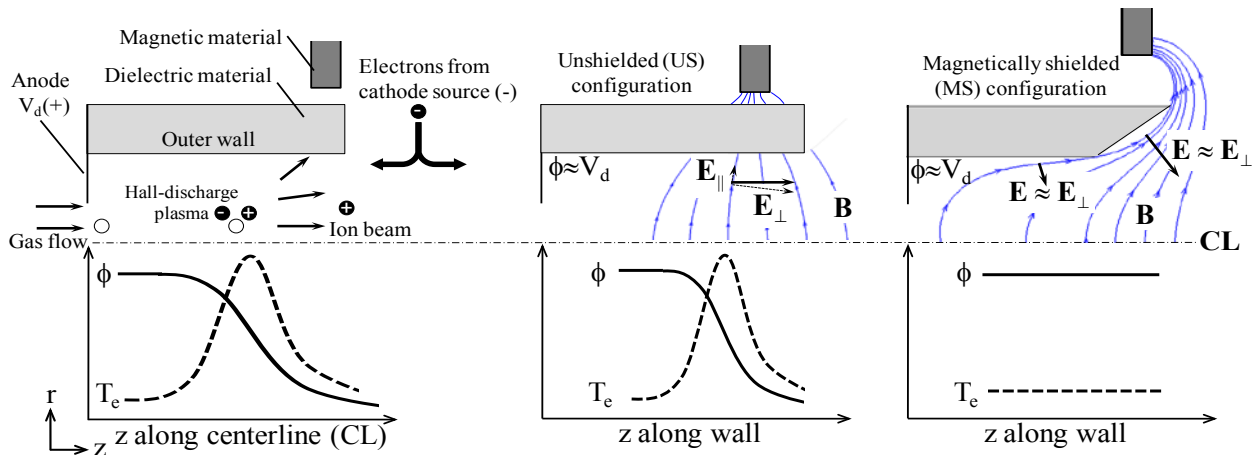

Fig. 1. *Schematics of the upper half of the annular acceleration channel in a typical magnetic-layer Hall thruster (top) and typical profiles of ϕ and T_e (bottom) established during ion acceleration. Left: Basic features of the accelerator and typical profiles along the CL. Middle: Representative magnetic field lines and profiles along the wall in a US configuration. Right: Representative magnetic field lines and profiles along the wall in a MS configuration. The line that extends deepest into acceleration channel and runs closest to the channel wall without crossing shall be called the "grazing line."*

American Institute of Aeronautics and Astronautics

B. **Numerical Simulations**
    1. Methods
    Since the preliminary numerical simulations of Phase I[12] a number of model improvements have been completed that allowed for a series of more accurate simulations of the H6, in both configurations. We present the results of these simulations in this section. The improved accuracy comes largely by way of an experimentally-guided non-classical electron collision frequency, the theoretical principles of which have remained elusive for decades. Specifically, by contrast to the Phase-I work during which only near-plume measurements existed, the Phase-II experimental campaign provided plasma measurements inside the acceleration channel. These new measurements in turn provided insight about the spatial variation of the collision frequency in this region. Therefore, in the present simulations the location of the acceleration zone and the plasma gradients that form it are known with better accuracy. We have found that these more accurate plasma solutions have not jeopardized in any way our original theoretical predictions[12] about the effects of magnetic shielding on the near-wall plasma and, in turn, on the erosion rates.

    The numerical simulations have been performed with the Hall2De code,[10,18] a two-dimensional (2-D) computational solver of the conservation equations that govern the evolution of the partially ionized gas in these thrusters. The governing equations, numerical methodology, various thruster simulations and comparisons with measurements have been presented elsewhere.[9,10] Here, we provide only a brief overview of the code for completeness. In Hall2De excessive numerical diffusion due to the large disparity of the transport coefficients parallel and perpendicular to the magnetic field is evaded by discretizing the equations on a computational mesh that is aligned with the applied magnetic field. The MFAM capability in Hall2De was largely motivated by the need to assess the life of Hall thrusters with complicated magnetic field topologies. Shown in Fig. 2-left is a schematic of the computational domain used in the H6 simulations with naming conventions of various thruster components and boundaries. A photograph of the thruster operating in a vacuum facility at JPL is shown in Fig. 2-right. The MFAM spans a computational domain in r-z geometry that extends several times the thruster channel length in the axial direction, and encompasses the cathode boundary and the thruster CL. The numerical solution of the conservation equations for the heavy species is performed without invoking discrete-particle methods. The evolution of the (collisionless) neutral species is computed using line-of-sight formulations that account for ionization.[18] Ions are treated as an isothermal, cold (relative to the electrons) fluid, accounting for the drag force and the ion-pressure gradient. Up to triply-charged ions and up to four distinct ion fluids can be included in Hall2De. In the H6 simulations presented here three charge states were accounted for but all ions were considered to be part of a single fluid. The electron population in Hall2De is treated also as a fluid. The solution of the electron energy conservation equation provides T_e. Ohm's law is solved in the frame of reference of the magnetic field with the electrical resistivity accounting for contributions from collisions of electrons with all other species. It has also been argued that the diffusion of electrons in Hall thrusters is enhanced in a non-classical manner by plasma turbulence (e.g. see e.g. see Refs. 19, 20, 21, 22). In numerical simulations this enhancement has typically been modeled using an effective or "non-classical" collision frequency. In this article we shall denote this collision frequency as ν_α. In Hall2De we impose a so-called transport coefficient function $f_\alpha(r,z)$ and define $\nu_\alpha \equiv f_\alpha \omega_{ce}$. In the present simulations f_α has been guided by plasma measurements that span both the acceleration channel interior and the thruster plume region. The conservation equations for the electrons are closed with boundary conditions (BC) at all surfaces shown in Fig. 2-left. The channel (ring) walls and the thruster front plate are dielectric boundaries. At the anode we impose sheath BCs for the electron current density normal to the anode.[12] At the cathode boundary the neutral particle flux, ion flux, plasma potential and electron temperature are specified. For all dielectric-wall boundaries a zero-current condition is imposed. At these surfaces the BC for the convective heat loss follows the formulations of Hobbs and Wesson[23] for the potential drop in a sheath with secondary electron emission. The far plume solution is subject to outflowing BCs. The energy equation is solved in a semi-implicit fashion; the thermal conduction term is implicit whereas all other terms are evaluated explicitly. Current conservation, incorporating Ohm's law to solve for the electron current density, is also solved implicitly.
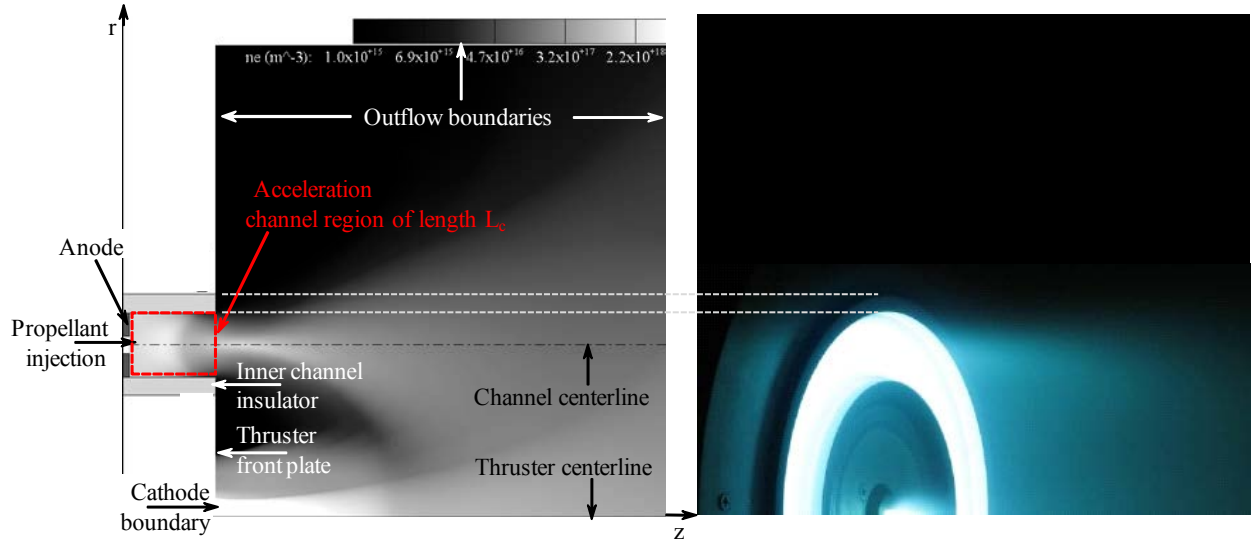
Fig. 2. *Left: Computational domain used in the numerical simulations of the H6 laboratory Hall thruster showing naming conventions for the various thruster components and boundaries that are cited throughout this paper. Right: Photograph of the thruster operating in a vacuum facility at JPL.*

Channel erosion in Hall2De accounts for contributions from Xe^+, Xe^{++} and Xe^{+++}. The sputtering erosion rate (ε) due to ion bombardment is given by,

$$\varepsilon = j_{i\perp} Y, \tag{I-3}$$

where the incident ion current density perpendicular to the channel wall, $j_{i\perp}$, is dependent on the ion number density (n_i) and the ion velocity (u_i) at the wall. The sputtering yield (Y) of the channel material is a function of the ion impact energy (K) and incidence angle (β). Because ions must traverse a sheath before striking the wall, the total impact energy is the sum of the kinetic energy $K_i = \frac{1}{2} m_i u_i^2 / q_i$ (expressed in units J/C) ions of mass m_i have acquired in the plasma upon entrance to the sheath, and the sheath potential energy denoted as $\Delta\phi$. That is,

$$j_{i\perp} = j_{i\perp}(q_i, n_i, u_{i\perp}) \qquad Y = Y(K_i + \Delta\phi, \beta). \tag{I-4}$$

The potential energy $\Delta\phi$, transformed to ion kinetic energy as the plasma ions are accelerated inside the sheath towards the solid material, is computed based on the solution to the 1-D sheath equations in the presence of secondary electron emission. Hobbs and Wesson[23] showed that the sheath equations for this problem consist of a system of three non-linear equations for the electric field, sheath potential and ion Mach number. For ease of computation in the numerical simulations we employ a fit[24] to the Hobbs and Wesson solution such that $\Delta\phi = \Delta\phi(T_e)$. Thus, direct comparisons of T_e between wall-probe measurements and near-wall simulations results (to be discussed later in this article) provide insight not only about the heating of the electrons but also about the sheath energy of ions. In the numerical simulations the vertex-centered ion velocities and the element-centered n_i at each computational element adjacent to the wall boundary are used to determine the total impact energy $K = K_i + \Delta\phi$ and angle β. Then the sputtering yield is determined as follows:

$$Y = f_\beta(\beta) f_K(K), \tag{I-5}$$

where the fitting functions $f_K(K_i+\Delta\phi)$[25] for the energy dependence at zero angle of incidence and $f_\beta(\beta)$[26] for the angle dependence are given by

$$f_\beta(\beta)=1+c_0[1-\cos(c_1\beta)]^{c_2} \qquad f_K(K)=\begin{cases} c_3\left[1-\left(\dfrac{K_T}{K}\right)^{2/3}\right]\left(1-\dfrac{K_T}{K}\right)^2 & K \geq K_T \\ 0 & K < K_T \end{cases} \qquad (I\text{-}6)$$

The two functions are plotted in Fig. 3. Also plotted in Fig. 3-right for comparison is a simplified model of the semi-empirical law proposed by Yamamura and Tawara (Y&T)[27] and used in the Phase-I preliminary simulations[12] as well as in simulations of other thrusters.[28] Of significance here is the increase in the value of K_T from 5.1 V (used in Phase I) to the range 25-50 V. The latter has been used in the present work. This increase was prompted in part by the Phase-I simulations which predicted unreasonably high erosion of the channel walls far upstream of the channel exit where such erosion has never been observed. These erroneous erosion trends persisted also in the experimentally-validated plasma simulations that followed the Phase-I work. Thus, a new fitting function f_K was sought.
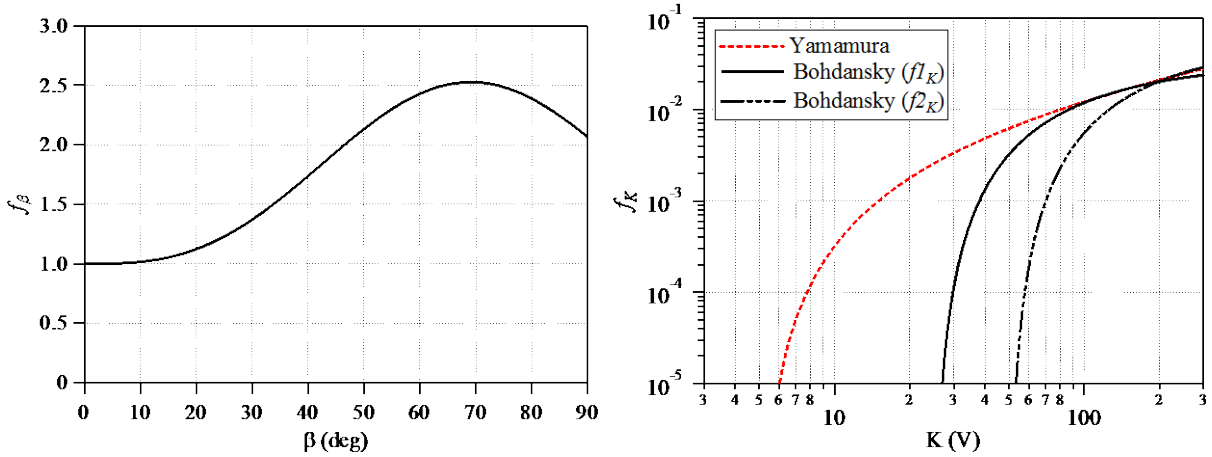

Fig. 3. *Fitting functions for the sputtering yield of the BN channel material used in the H6 (see Eqs. (I-5) & (I-6)). Left: The coefficients for the angular dependence function f_β (Eq.(I-6)-left) are c_0=0.52663, c_1=2.60506, c_2=1.53462. Right: Energy dependence function f_K. Both models by Bohdansky[25] (Eq.(I-6)-right) $f1_K$ and $f2_K$ have been used in the present simulations. The coefficients are c_3=0.035, K_T=25 for $f1_K$, and c_3=0.06, K_T=50 for $f2_K$.*

For the boron-nitride (BN) material used in the H6 channel insulators there are only limited measurements of the sputtering yield, most of which provide values for energies that exceed 100 V. The most recent data for energies <100 V have been produced by Rubin et al.[29] Based on a comparison of the fitting function f_K (Fig. 3-right) with Rubin's data, Shastry[30] showed that the measured sputtering yield values were higher by factors ranging 2-5 for energies >100 V. With a new set of fitting functions based on Rubin's data, Shastry suggested that the sputtering yield exhibits a steeper fall at low energies, dropping below 10^{-4} between 30-45 V instead of the ~10 V predicted by the Y&T model with K_T=5.1 V. However, Rubin *et al.* acknowledged that their values are higher than published data and no explanations were provided for this discrepancy. In a series of sensitivity simulations and comparisons with profilometry measurements we have found that $25 \lesssim K_T \lesssim 50$ V covers the range within which the true threshold most likely resides. This is also in agreement with the conclusions of Shastry.[30] Therefore, since a single value of the sputtering yield threshold remains unknown, in the present work we provide results for the two assumed limits, 25 V and 50 V. Regarding the functional form of f_K we found that the function proposed by Bohdansky[25] (Eq. (I-6)-right) allows us to attain these higher thresholds while retaining close agreement with the values of the Y&T model at K≳ 200 V where yield data are not as scarce. The two functions $f1_K$ and $f2_K$ are plotted in Fig. 3-right. It is noted that when K<K_T, ε is set to zero in Hall2De.

American Institute of Aeronautics and Astronautics

2. Numerical Simulation Results

Compared to the simulations presented in our Phase-I preliminary design work,[12] a noteworthy advancement of the present simulations is associated with the location of the acceleration zone relative to the channel exit. Specifically, the acquisition of both internal and wall-probe data in the Phase-II experimental work[16] allowed for the resolution of the steep-gradient (acceleration) region of the thruster, which subsequently provided detailed guidance on the transport coefficient function f_α. The revised simulations now show the plasma inside the channel displaced downstream by $\Delta z/L_c \approx 0.18$ compared to the solution obtained in Phase I. This displacement has been found to be too small to alter our overall predictions on the >order-of-magnitude reductions of the channel erosion. As originally argued in previous publications[10,12] this is because magnetic shielding is relatively insensitive to spatial displacements of this magnitude in the interior plasma. We elaborate further on this subject in ensuing sections of this paper.

In this section we present results from the new (Phase-III) series of numerical simulations of the H6 thruster in both thruster configurations. These results are then used to determine all properties along the channel walls that are relevant to erosion. As shown in Fig. 2, the H6 channel geometry is relatively simple and the hollow cathode is located at the thruster CL, which allows for unambiguous one-on-one comparisons with the 2-D axisymmetric results of Hall2De. All simulations have been carried out at discharge voltage and current of 300 V and 20 A, respectively. The thruster experiments were performed at these same discharge conditions. The anode flow rate was somewhat different but these differences have been found to be too trivial to affect the overall comparison of the quantities that are pertinent to erosion. In the US configuration the anode flow rate was 0.5 mg/s (2.6%) higher in the experiments, whereas in the MS configuration it was 0.85 mg/s (4.4%) lower. Referring to Fig. 2, the maximum axial and radial dimensions of the computational domain were $(z/L_c)_{max}=6.25$ and $(r/L_c)_{max}=5.5$, respectively where L_c denotes the length of the acceleration channel region. In the MS configuration L_c is defined as shown in Fig. 4-bottom-right. The MS channel was ~2 mm (~5%) shorter than the US channel.

Table 1. *Contributions of the different ion charge states to the erosion rates near the exit of the <u>outer wall</u> (z/Lc≈0.98), as determined from the numerical simulations. For the erosion rates the $f1_K$ model was used.*

Thruster Configuration:	Unshielded (US)			Magnetically Shielded (MS)		
Charge State	$j_{i\perp}$ (C/hr/mm^2)	K (V)	ε (mm/kh)	$j_{i\perp}$ (C/hr/mm^2)	K (V)	ε (mm/kh)
Xe$^+$	8.38×10^{-2}	194	4.19×10^0	2.38×10^{-2}	20.7	0.0*
Xe^{++}	3.64×10^{-2}	121	1.30×10^0	3.99×10^{-4}	19.5	0.0*
Xe^{+++}	4.44×10^{-3}	113	1.48×10^{-1}	6.44×10^{-7}	20.8	0.0*

*Erosion rate set to zero in Hall2De when $K<K_T$.

Table 2. *Contributions of the different ion charge states to the erosion rates near the exit of the <u>inner wall</u> (z/Lc≈0.98), as determined from the numerical simulations. For the erosion rates the $f1_K$ model was used.*

Thruster Configuration:	Unshielded (US)			Magnetically Shielded (MS)		
Charge State	$j_{i\perp}$ (C/hr/mm^2)	K (V)	ε (mm/kh)	$j_{i\perp}$ (C/hr/mm^2)	K (V)	ε (mm/kh)
Xe$^+$	8.52×10^{-2}	248	4.75×10^0	4.72×10^{-3}	43.8	2.40×10^{-2}
Xe^{++}	3.97×10^{-2}	157	1.75×10^0	8.95×10^{-5}	46.7	5.82×10^{-4}
Xe^{+++}	6.40×10^{-4}	162	2.88×10^{-1}	1.54×10^{-7}	49.1	1.19×10^{-6}

The 2-D simulation results in the vicinity of the acceleration channel are compared in the US and MS configurations in Fig. 4. Results that are pertinent to wall erosion also are plotted in Fig. 5. Tables 1 and 2 compare the contributions of each charge state to the erosion near the channel exit ($z/L_c \approx 0.98$). We found no major differences between these Phase-III results and those reported in our Phase-I work regarding the ability of the magnetic shielding field topology to alter favorably the near-wall properties. The effect of magnetic shielding on the plasma potential is evident in Fig. 4-top. We compute only a 4-15 V reduction along the MS diverging walls compared to a drop of 250-260 V along the US walls near the channel exit. K_i is therefore lowered significantly in the MS configuration; Fig. 5-top-left and Table 1 show reductions as high as ~one order of magnitude near the channel exit of the outer wall. Smaller reductions are computed along the inner wall.
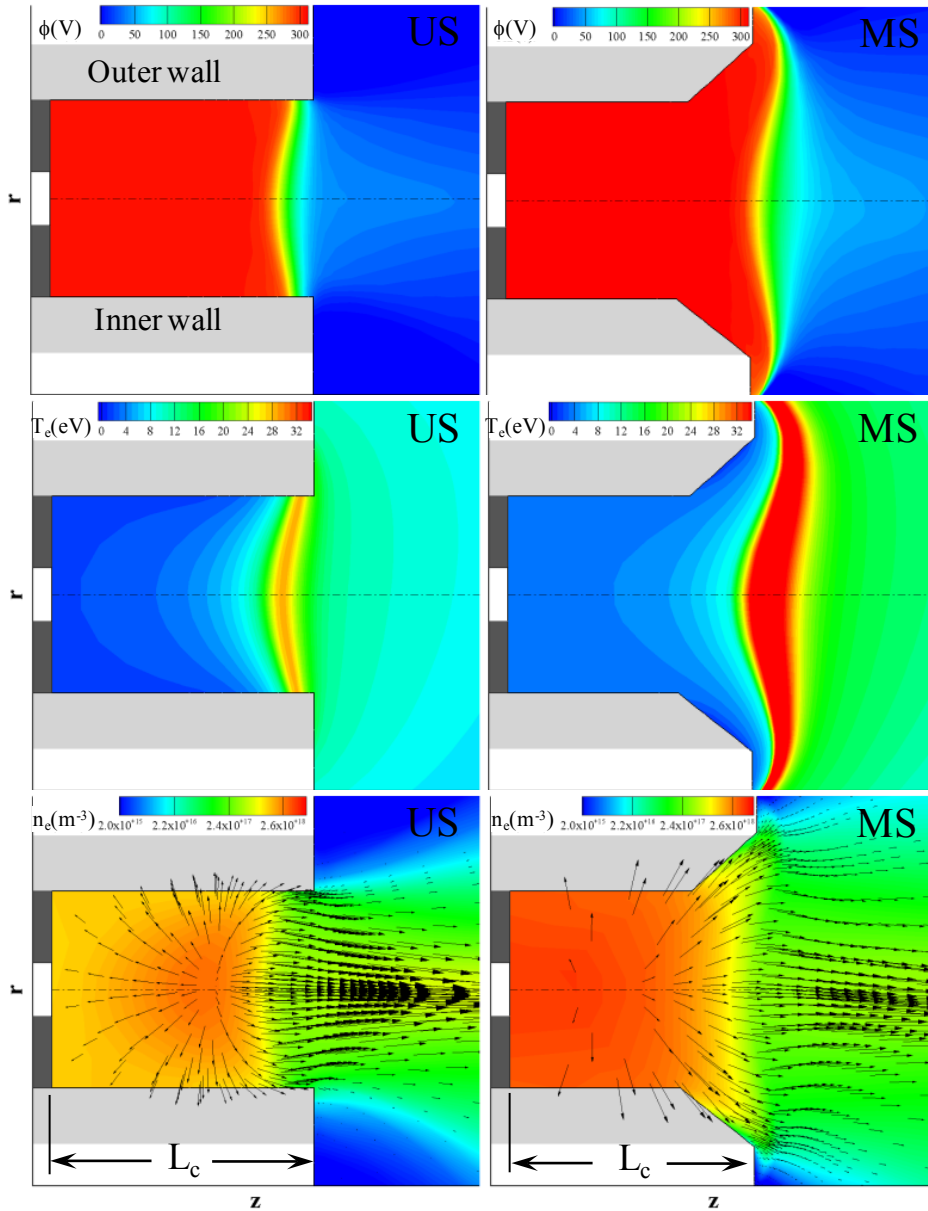

Fig. 4. *2-D numerical simulations of the Hall-discharge plasma in the US (left) and MS (right) accelerator configurations. Top: Plasma potential. Middle: Electron temperature. Bottom: Electron number density overlaid by vectors of singly-charged ion current density.*

American Institute of Aeronautics and Astronautics

If **B**-lines are isothermal, an assumption that is to be confirmed in Sec. II.A.1, then those that graze the corner formed by the cylindrical and diverging sections of the MS channel must also be associated with low T_e because they extend deep into the acceleration channel where the electrons are cold (Fig. 1-right). Indeed, the comparison of the two configurations in Fig. 4-middle shows a significant reduction of T_e in these highly shielded wall regions. Because T_e is reduced, a decrease of the sheath fall is also induced. In the last ~20% of the channel we compute a reduction in the sheath energy of about 4-10 times that in the US configuration (Fig. 5-top-right).

Finally, because near the MS walls $E_{\parallel}$ is practically eliminated, ion acceleration occurs mostly away from the walls. This leads to lower wall-incident ion flux. Referring to Fig. 5-bottom-left, for Xe^+ $j_{i\perp}$ near the channel exit is found to be 3.5-18 times lower in the MS configuration. In regions where the MS fluxes begin to become comparable to the US fluxes, the ion energy has been found to be below the lowest energy threshold assumed in the simulations (25 V). In fact $K<K_T$ has been found to hold true along the whole MS outer wall.
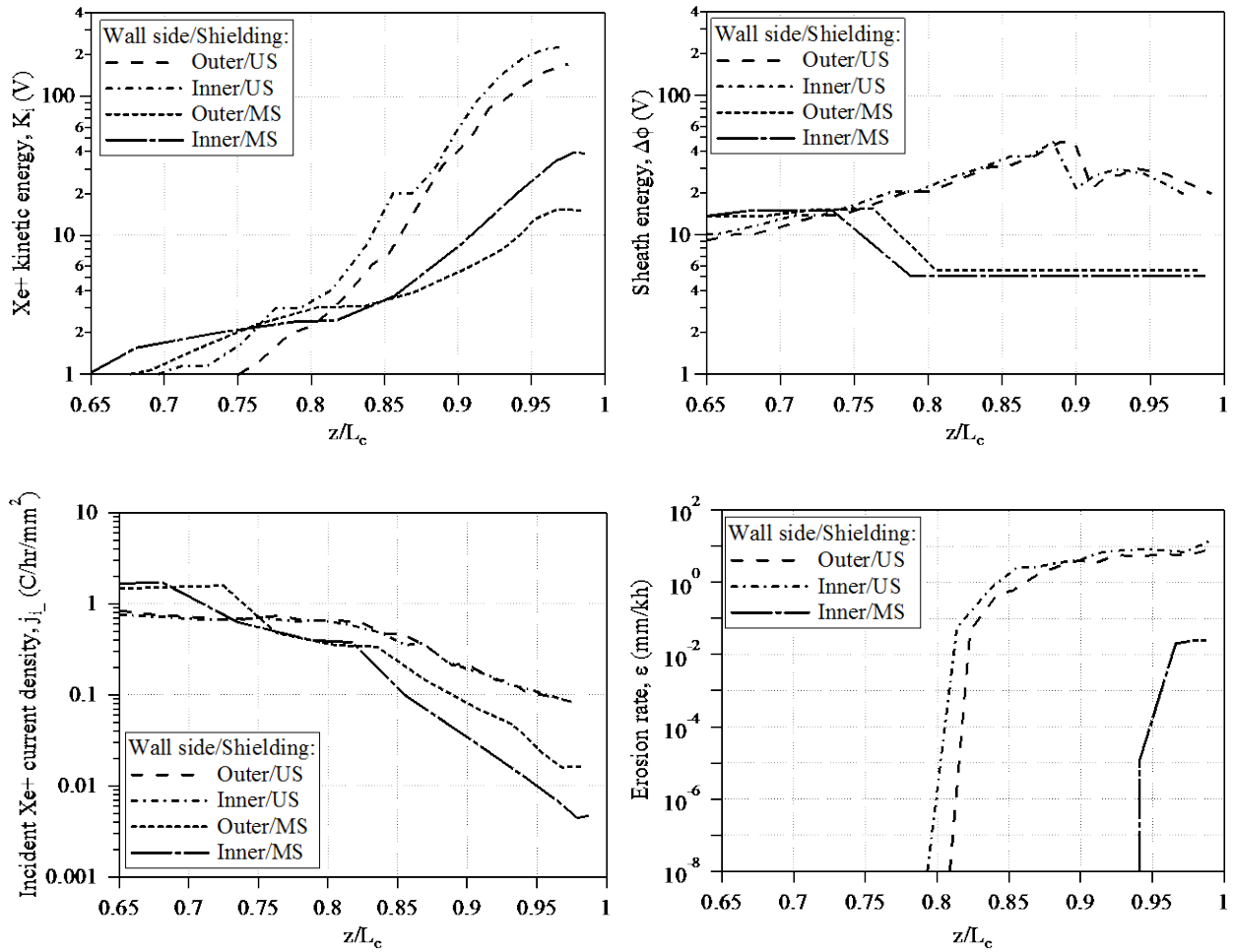

Fig. 5. *Numerical simulation results along the channel walls. Top-left: impact kinetic energy of Xe^+. Top-right: Sheath energy of Xe^+. Bottom-left: Current density of incident Xe^+. Bottom-right: Total erosion rate (accounting for all three ion charges states). The total ion energy at the MS outer wall is below the threshold (25 V) for sputtering and thus no erosion is computed.*

American Institute of Aeronautics and Astronautics

II. Validation of the Theory by Experiments

It was emphasized early in the program that achievement of reduced erosion rates in the laboratory alone, albeit necessary, could not be sufficient evidence to complete the demonstration of the technique. Proof of the physics that led to such reductions would also have to be established. Thus, our objective was twofold: (1) to demonstrate significantly reduced erosion rates in the laboratory <u>and</u> (2) to demonstrate that the near-wall properties were modified according to the theoretical predictions. Accordingly, in addition to erosion diagnostics the experimental campaign following Phase I included several plasma diagnostics to validate the theory. A total of 16 different diagnostics were used, a detailed description of which is provided in our companion paper.[16] In this section we present comparisons with plasma measurements from (1) near-field plume probes, (2) reciprocating probes injected axially in to the discharge chamber, and (3) flush-mounted wall probes. For erosion, we compare our simulation results with measurements from (1) profilometry, using a coordinate measuring machine (CMM) technique and (5) a quartz crystal microbalance (QCM) mounted near the thruster to determine the back-sputter rate of carbon. Finally, due to the significance of the applied magnetic field we also report on comparisons from interior and exterior measurements using a 3-axis gaussmeter. All the experiments were performed in a 3-m diameter by 10-m long vacuum facility at JPL, at a discharge voltage and power of 300 V and 6 kW, respectively. We focus here exclusively on comparisons that are relevant to magnetic shielding physics because only small differences in thruster performance were measured between the two configurations. Using %(US-MS)/US to define performance variations, thrust, total efficiency and total specific impulse changed by 4.2%, 1.7% and -2.6%, respectively. A more extensive comparison of the measured performance in the two configurations is reported in our companion paper.[16]

A. **Plasma and magnetic field**
    1. <u>Isothermal properties of the magnetic field lines</u>

Conservation of the electron temperature is a fundamental property of the lines of force in the thrusters, as deduced originally by Morozov et al.[2,3] It has been argued that this assumption may break down in regions near the hollow cathode due to the increased collisionality of the electrons there.[12] The validity of the assumption inside the acceleration channel also has been questioned.[31] Because isothermality of the lines is critical in magnetic shielding, we present here evidence that this property is indeed preserved in the H6 acceleration channel. The locations of the wall probes mounted along the channel during the experiments with the US configuration are depicted in Fig. 6-top. The left plot shows also magnetic field lines that intersect the locations of the wall probes at the inner wall and terminate at some points along the outer wall. The magnetic field shown here was the product of a direct measurement with a 3-axis gaussmeter. Noted is that the intersections of these lines with the outer wall do not coincide with the locations of the outer-wall probes. The right plot in Fig. 6-top shows the same arrangement but with the lines now starting from the locations of the outer-wall probes. The intent here is to compare T_e measured directly by the probes at one side of the wall with those extrapolated along the lines of force from the opposite side of the wall. If the lines are isothermal then the two sets of data should follow closely the same T_e trend with axial position. Indeed, we find this to be true as shown in Fig. 6-bottom. It is noted that although the locations of all five probes used in the experiments (on each wall) are depicted in Fig. 6-top not all probes produced a T_e measurement.

    2. <u>Comparison of simulation results with plasma measurements at the channel CL</u>

A system of fast-moving reciprocating probes was used to obtain plasma measurements inside the acceleration channel. Internal measurements have been a critical part of the validation effort because they provided information about the steep plasma gradients in the acceleration region. In turn, this information was used in the simulations to guide the spatial variation of f_α. Shown in Fig. 7 are measurements of T_e and ϕ along the channel CL using Langmuir and emissive probes, respectively. A description of the diagnostics is provided in Ref. 16. To reduce the spatial uncertainty associated with the fast-moving probes, the final axial location of the CL data was determined based on the location of the wall probe data

and the measured magnetic field. Specifically, referring to Fig. 7-left, the maximum value of T_e measured by the wall probes was extrapolated along its corresponding magnetic field line onto the CL. Then the axial location of the maximum T_e measured at the CL was relocated to equal to the location inferred from the wall-probe extrapolation. The remaining CL data were displaced by the same distance from the original location recorded by the fast-probe instrument. This calibration of the CL data assured their consistency with the wall-probe data. Henceforth, we shall denote this as the calibrated set of CL data. Naturally, the flush-mounted wall probes were chosen to guide the location of the fast-moving probe data at the CL because the spatial uncertainty of the former is negligible.
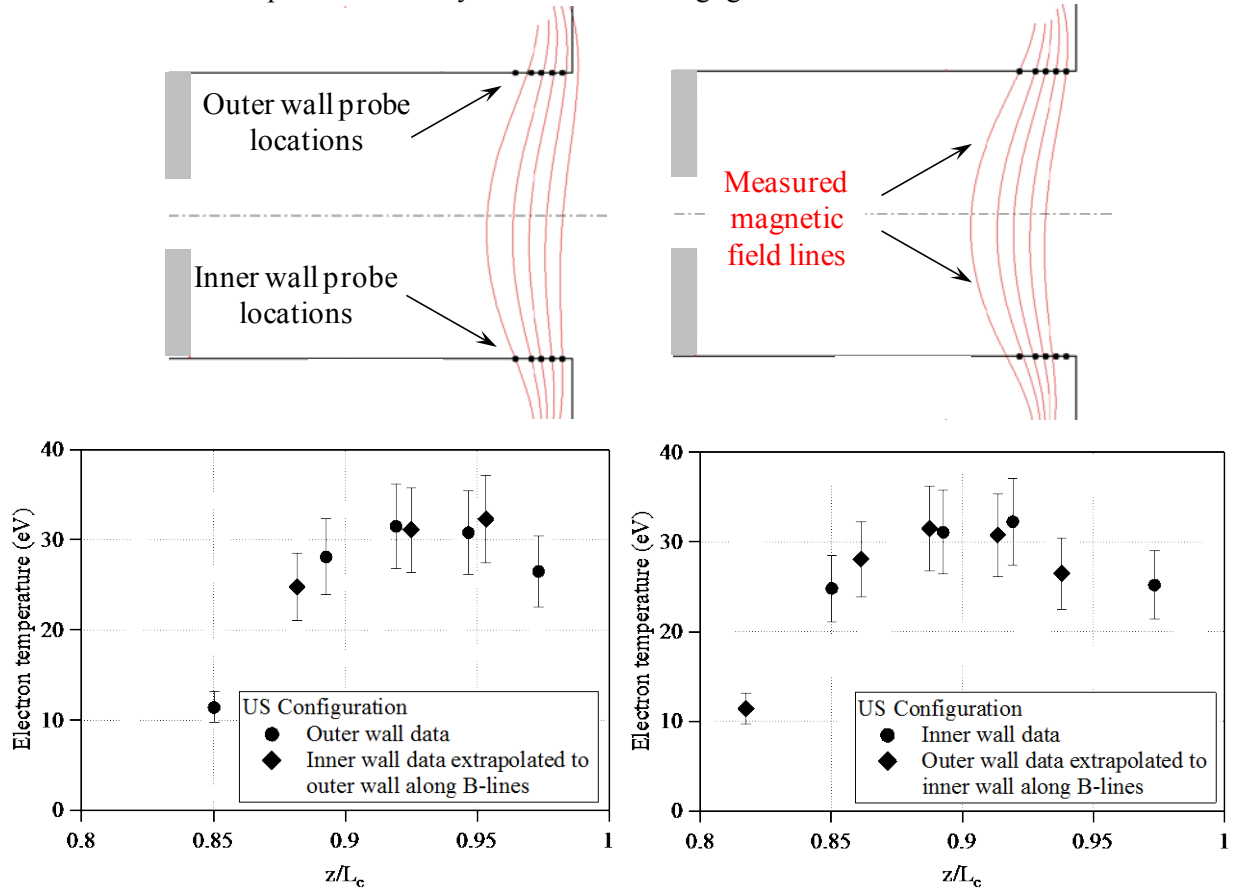

Fig. 6. *Evidence supporting the conservation of T_e along magnetic field lines in the acceleration region of the H6 thruster. Top-left: Measured magnetic field lines intersecting the inner wall probes and terminating on the outer wall. Top-right: Measured magnetic field lines intersecting the outer wall probes and terminating on the inner wall. Bottom-left: Comparison of T_e measured directly by the outer-wall probes with that measured by the inner-wall probes and extrapolated to the outer wall along magnetic field lines. Bottom-right: Comparison of T_e measured directly by the inner-wall probes with that measured by the outer-wall probes and extrapolated to the inner wall along magnetic field lines.*

The determination of the location of ϕ at the CL is more challenging because the lines of force are not equipotential. Thus, measured values from the wall probes alone cannot be used directly to guide the location of ϕ at the CL unless they are is some guidance from the numerical simulations. Indeed, this is what was done here and the resultant comparison is shown in Fig. 7-left. It is worthwhile noting that the maximum T_e in the profiles of Fig. 7-left is within 0.5 mm ($\Delta z/L_c \sim 0.01$) of the maximum $E_\perp$. This is important because maximum heating of the electrons is expected to occur near the location where the resistive contribution ηj_e^2 to the work done by the electric field $E \cdot j_e$ is also a maximum. This typically occurs near the location of maximum $E_\perp$. The precise location of the maximum T_e is of course dependent

upon the balance between resistive heating and all the mechanisms that remove heat locally by convection, diffusion and volumetric cooling. Even with the wide range of diagnostics that has been performed in our experiments, the details of such balance can be determined self-consistently only by numerical simulation. A comparison between the calibrated and un-calibrated CL traces from the fast-moving probes in the US configuration yields an uncertainty in their axial position of 3.6-5.8 mm ($0.09 < \Delta z/L_c < 0.14$).

In the MS configuration the topology of the magnetic field is designed in a manner that eliminates impingement of lines onto the channel walls (see Fig. 1-right). Thus, the magnetic field and the wall probe measurements in this configuration cannot be used to calibrate the CL data. However, a comparison between the un-calibrated CL traces in the two thruster configurations revealed that the distance between the axial locations of the T_e maxima was within ~1 mm of the distance between the magnetic field maxima. Specifically, based on the T_e and ϕ probe traces, it was found that relative to the US configuration the plasma in the MS configuration was displaced downstream by about the same distance (within 1-2 mm) that the maximum magnetic field was displaced. In the MS configuration the downstream displacement of the magnetic field maximum is a natural and expected consequence of the design, caused by the addition of magnetic flux near the walls needed to form the shielding topology. The consequent displacement of the plasma is not surprising since the main accelerating body force on the ions, $\mathbf{E}_\perp/q_i$, is proportional to B^2. Hence, the final axial location of the CL probe data in the MS configuration was determined based on the CL data in the US configuration (the position of which was calibrated based on the wall-probe data) and the location of the maximum magnetic field at the CL. A comparison between the calibrated and un-calibrated CL traces from the fast-moving probes in the MS configuration yields an uncertainty in their axial position of 3.6-7.9 mm ($0.1 < \Delta z/L_c < 0.21$). Here, it must be emphasized that this uncertainty in the axial location of the plasma is of little significance on magnetic shielding. This is because the plasma properties along the walls are driven largely by (1) the plasma properties near the anode and, (2) the specific magnetic-shielding field topology. We have confirmed this insensitivity by performing additional numerical simulations of the MS configuration that displaced the plasma by several millimeters compared to the position depicted in Fig. 7-right. The results of these simulations are discussed in greater detail in Sec. II.B.2.
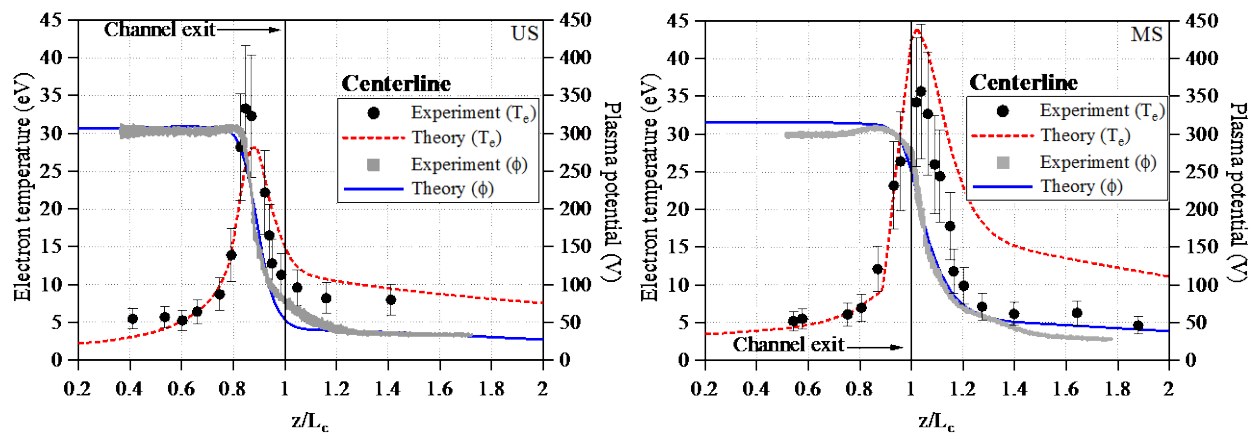

Fig. 7. *Comparison between numerical simulations and probe data along the channel CL in the US (left) and MS (tight) configurations. The measurements were conducted using a fast-moving probe system.*[16]

The resolution of the steep-gradient regions by the internal probe measurements provided information about the spatial variation of ν_α inside the channel we did not have in Phase I. This new information then allowed us to obtain a plasma solution that is now within the experimental uncertainties for the majority of the channel interior in both thruster configurations, as illustrated in Fig. 7. In the exterior, the comparison with the near-plume data is also very good with the exception of T_e in the MS configuration (Fig. 7-right). We argue that in the simulations the enhanced heating of the electrons in this region

occurred largely due to an underestimated plasma density at large ion-divergence angles. To better illustrate this we refer the reader to Fig. 4-middle and -bottom. In the US configuration we point out that the (typical) high-temperature zone is seen to be formed by a set of magnetic field lines that intersect the channel walls (Fig. 4-middle-left). In this configuration then maximum electron heating occurs inside the channel where the plasma density is on the order of 2×10^{17} m^{-3} along the full extent of the magnetic field lines including regions near the walls where the lines terminate. In contrast, the MS topology eliminates (by design) the impingement of the magnetic field lines onto the interior surfaces of the channel walls, which forces the formation of the high-temperature zone downstream of the channel exit (Fig. 4-middle-right). The consequence is that the magnetic field lines that form the hot zone now terminate at the thruster front plate and vertical outflow boundaries (Ref. Fig. 2), where the density has fallen by about two orders of magnitude. Hence, in the US case, significantly more cooling of the hot electrons occurs near the walls due to higher ionization, excitation and energy flux losses to the walls. In the MS configuration, though the plasma density at the channel CL is comparable to that in the US configuration, the much lower densities at the top and bottom ends of the hot zone (Fig. 4-bottom-right) allow for lower electron energy losses there, which lead to higher T_e. There are at least two reasons for the underestimated plasma density in the regions of high ion divergence angles: (1) well-known shortfalls of the hydrodynamic numerical scheme to capture accurately the expansion of the ions in these regions and, (2) the assumption of a single ion population. In regards to the second, we have found (in soon-to-be-published work) that the single-fluid approximation for ions in the near plume fails due to the presence of slow ions from the hollow cathode. These cathode ions constitute a distinct population from the thruster ions. We have found from simulations of the US configuration that accounting for cathode ions separately, which is within the simulation capabilities of Hall2De, leads to higher plasma densities in the high-angle expansion regions near the channel exit, and to higher electron energy losses. Simulations of the MS configuration with multiple fluids have not yet been performed. Of course, other mechanisms possibly associated with the unknown transport of the electrons in these regions, and/or other energy loss not presently accounted for in the simulations cannot be excluded as source(s) of the discrepancy in T_e. This subject has been rendered beyond the scope of this work because, as illustrated in Fig. 4-middle-right, the MS topology near the chamfered walls continues to serve as an effective thermal insulator to hot electrons. Thus, even if the characteristic T_e of the hot-electron zone in the simulation was lower this would have had no impact on the near-wall T_e.

   3.   Comparison of simulation results with plasma measurements at the channel walls

   One of the most critical aspects of the validation of magnetic shielding is the confirmation of the predicted plasma properties along the walls. In this section we present a series of comparisons between numerical simulations and measurements from the wall-imbedded probes. The location of the probes was shown in Fig. 6. More information about the probe diagnostics and data analysis is provided in our companion paper.[16] In Fig. 8 we compare computed and measured T_e (left) and ϕ (right) at the outer (top) and inner (bottom) channel walls. Referring first to the comparisons in the US configuration, we find good correlation with the qualitative trends from the probes. Of particular importance is the agreement on the location where ϕ begins to decrease appreciably from the near-V_d values (Fig. 8-right), since it is beyond this point where ions near the walls begin to acquire significant kinetic energy. This is also the region where ions can acquire additional energy from the sheath as suggested by the rise T_e there (Fig. 8-left). Hence, we expect this region of the walls to exhibit the highest erosion rates. Visual inspection of the rings after the thruster was tested in a vacuum facility confirms this expectation. A photograph of the US inner ring after 28 h of operation is provided in Fig. 9-left. The photograph shows a clear discoloration of the BN which is caused by the impingement of high-energy ions onto the surface. Along this "erosion band" the erosion rate exceeds the carbon deposition rate, which was measured during the test using a QCM mounted adjacent to the thruster. It is noted that the extent of the band was measured to be $z/L_c\approx0.1$ in agreement with the profiles of Fig. 8-right where increasing ion energy gains are found to exceed the sputtering yield threshold K_T (25-50 V) in this region. In Sec. II.B.1 we will show that the visual observation of the erosion zone is consistent also with profilometry measurements.
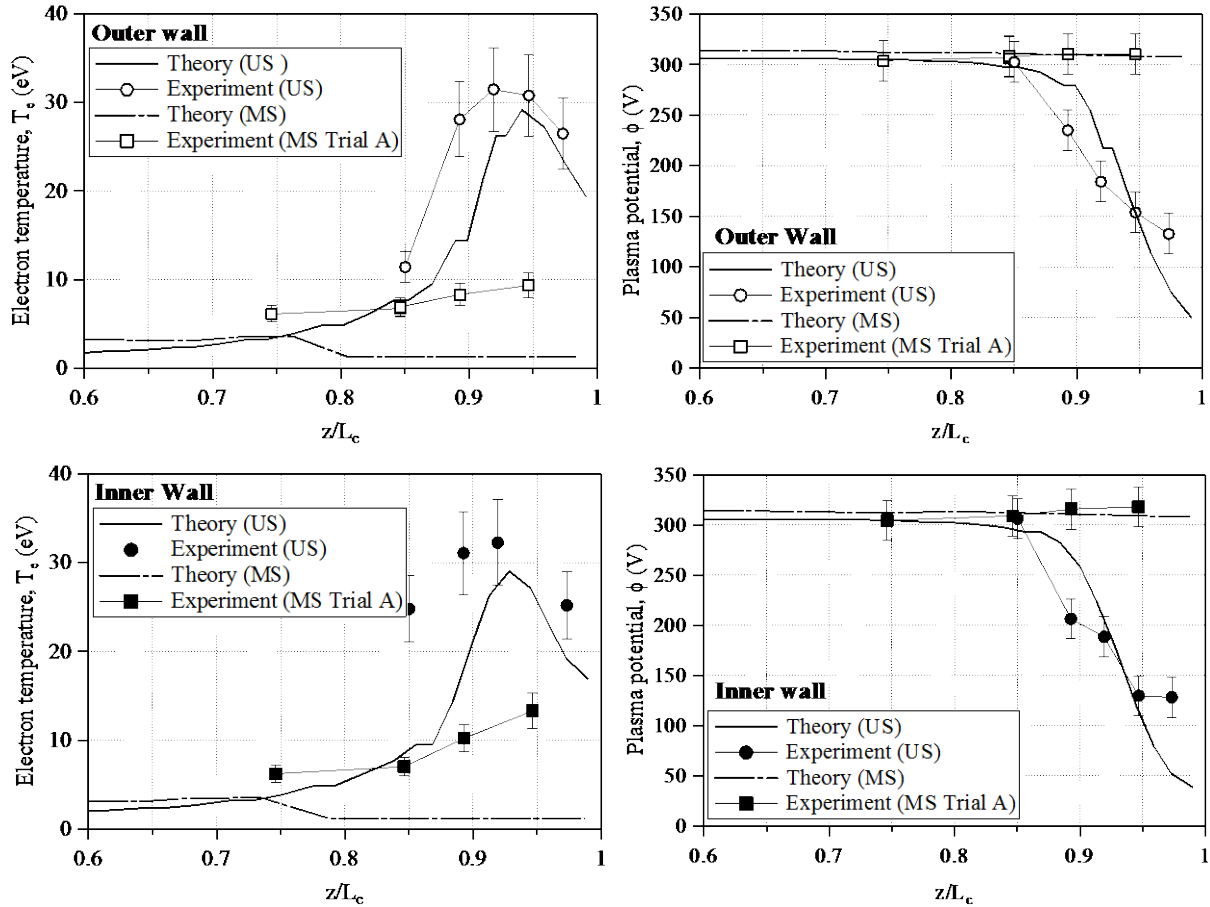
Fig. 8. *Comparisons between numerical simulations and data from flush-mounted wall probes. The comparisons validate the two primary effects of magnetic shielding on the near-wall plasma, as predicted by the theory: (1) sustainment of ϕ values that are near V_d and (2) colder T_e. The chamfered walls in the MS configuration span $0.72 \lesssim z/L_c \le 1$.*
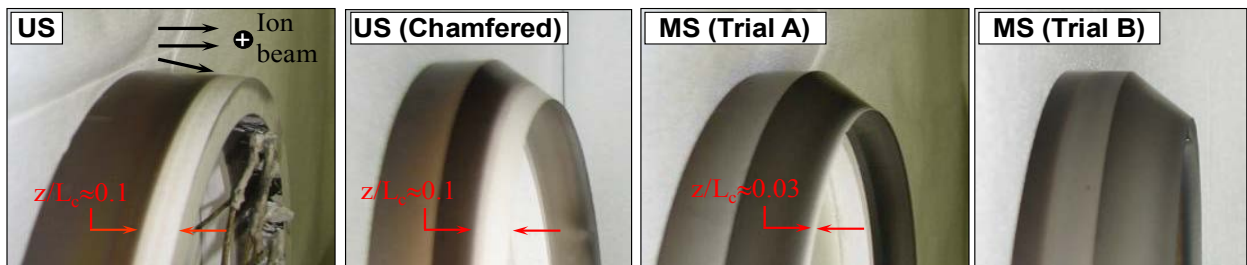

Fig. 9. *Photographs of the inner wall in the US and MS configurations after thruster operation in a vacuum facility. Dark-colored surfaces depict carbon-coated regions. Left: After 28 h of operation a white-colored band was visible in the US configuration that covered the last ~10% of the channel. The extent of this band correlated very well with profilometry measurements of the erosion zone. Left-middle: The MS channel geometry was tested for 10 h using the US magnetic field to demonstrate that chamfering of the channel without a properly design magnetic field does not reduce erosion. Right-middle: Approximately 97% of MS wall was coated with carbon in the first (Trial-A) experiments after 19 h. Some discoloration was visible in the last ~3%. Right: Repeat of the Trial-A experiments several months later. Upon conclusions of the 14-h test the discolored band was no longer visible.*

We observe also some marked differences in the US configuration between the theory and experiment. Specifically, it is apparent in Fig. 8-left that the measured temperature profile is broader than that from the simulation, more so along the inner wall than along the outer wall. We found that the main reason for this were discrepancies between the magnetic field used in the simulations and that applied in the experiment. Portions of the measured and simulated magnetic fields are compared for both configurations in Fig. 10. Noted in Fig. 10-left are the larger angles of incidence of the measured lines (shown in red) along the walls compared to those of the simulated lines (shown in black). That is, the distribution of the measured lines is broader along the walls compared to the simulated lines, which leads to a broader temperature profile since lines are isothermal in this region (as suggested by the results of Fig. 8-left). Also noted in Fig. 10-left is that the discrepancy between measured and simulated lines is greater along the inner wall than it is along the outer wall, which explains the larger discrepancies in the broadness of the T_e profiles depicted in Fig. 8-left. The reason(s) for the differences in the two magnetic fields is under investigation. Also underway are numerical simulations of the US configuration that employ directly the measured (rather than the simulated) magnetic field.

In the MS configuration the most significant comparison between simulations and measurements is that of ϕ (Fig. 8-right) because it demonstrates its sustainment to values close to V_d along the walls, as predicted by the theory (Fig. 1-right). The measured T_e also is seen to be lower along the walls, by about ~2.5-3 times compared to the measured values in the US configuration. Visual inspection of the MS rings after operation of the thruster for several hours supports this conclusion. As a preface to a more detailed discussion of wall erosion diagnostics and comparisons with the simulations in Sec. II.B.1, we present a photograph of the inner MS wall after 19 h of operation. The photograph labeled Trial-A shows clearly that the region of net carbon deposition spanned almost the entire wall. Some discoloration was observed in the last ~mm ($z/L_c \approx 0.03$) which is discussed in greater detail in Sec. [REF]. To demonstrate the significance of the magnetic field topology in magnetic shielding, a different experiment was conducted in which the MS rings were used but with the magnetic field topology of the US configuration. A photograph of the inner wall after completion of a 10-h experiment is shown in Fig. 9-middle left. Clearly visible is the same "erosion band" that was observed in the US configuration in Fig. 9-left with the same spatial extent of ~$0.1L_c$.

In the MS configuration Fig. 8 left-top (outer wall) and left-bottom (inner wall) show that the simulations consistently under-predict the measurement. A close-up view of the inner chamfered walls, where the largest discrepancy between theory and experiment is observed, is depicted in Fig. 11. The plot shows also the location of the wall probes overlaid by representative contours of constant T_e. Here, T_e was determined by Hall2De simulations using the simulated magnetic field (see Fig. 10-right). After accounting for a minor discrepancy in the axial extent of the channel (~1.2 mm) between the simulated and tested channel geometry, we found that the distance between the 13.3-eV contour and the probe location that yielded the same value of T_e is about 3.7 mm (Fig. 11). This distance would be reduced further if the BN underwent thermal expansion. Our estimates however do not predict that such expansion would exceed significantly ~1 mm. A simulation using the *measured* magnetic field in this configuration (red lines in Fig. 10-right) revealed an upstream shift of the 13.3-eV contour of <0.5 mm, which also is not sufficient to explain the observed discrepancies in T_e. Since the source(s) of the discrepancy between the measured and simulated magnetic fields (which exceed a few millimeters in some locations inside the channel) have not yet been identified, the possibility that a somewhat different topology was produced than the ones shown in Fig. 10, prior and/or during the testing, cannot be excluded. In fact, when the test was repeated several months later with the same MS geometry and magnetic circuit settings, and for approximately the same operation time, a different discoloration pattern was observed along the chamfered walls. We label this second test of the MS configuration as "Trial-B." A comparison of the last two photographs in Fig. 9 shows that the light-colored band that was visible in the Trial-A experiment (Fig. 9-middle-right) disappeared in the Trial-B experiment (Fig. 9-right). It is possible that lower erosion rates in this latter part of the chamfered wall occurred due to minor changes in the magnetic field relative to the wall in the Trial-B experiment, but this has not been confirmed. Other explanations such as heating mechanisms of the electrons not accounted for in the simulations cannot be excluded either. We argue

however that regardless of the specific source(s) of the discrepancy, the higher T_e measured by the wall probes does not alter significantly the effectiveness of magnetic shielding in this region because the major contribution to the erosion – the kinetic energy gained by ions in the plasma (compare Fig. 5 top-left with top-right) – was indeed found to be significantly lower in the MS configuration (Fig. 5 top-left). Therefore, the erosion rates are not expected to be significantly higher than expected in the MS configuration. This has been confirmed by direct measurements of the erosion rates. These measurements and their comparison with the simulated rates are the subject of the next section.
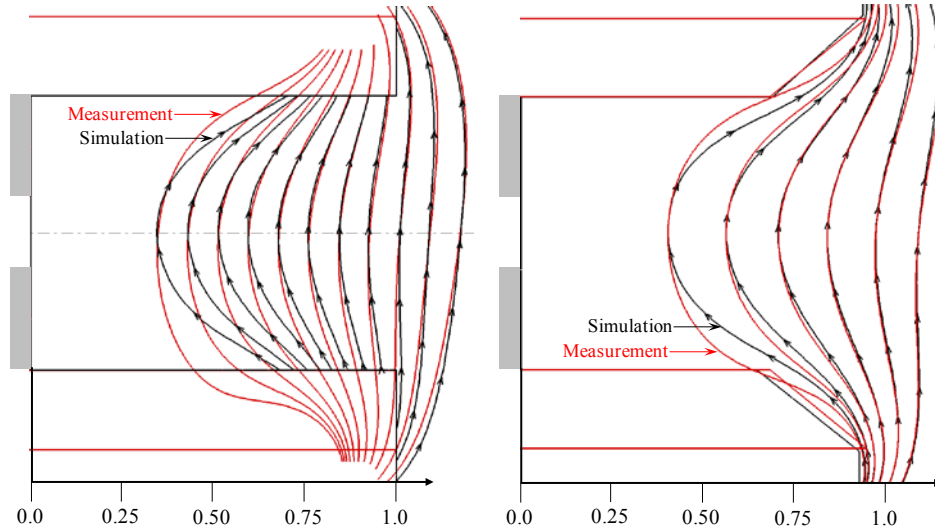
Fig. 10. *Comparison between the simulated (black streamlines) and measured (red streamlines) magnetic fields. The former was produced using a commercial software and has been used in all numerical simulations presented in this paper. The latter was measured upon the completion of the Phase-II experiments using a 3-axis gaussmeter. Also defined by red lines is the geometry of the tested thrusters. Outlined in black is the simulated geometry. Left: US configuration. Right: MS configuration.*
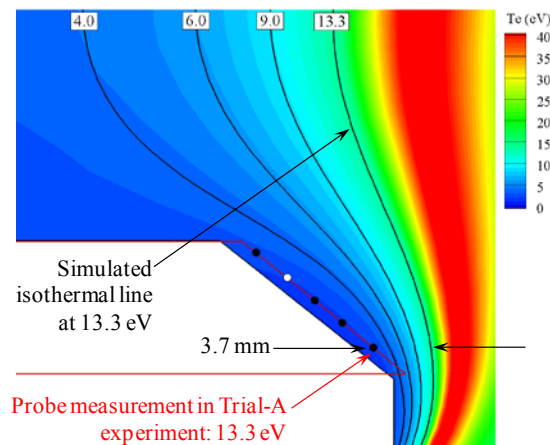

Fig. 11. *Numerical simulation showing contours of constant T_e in the vicinity of the inner MS wall. Also depicted are the geometry of the channel (red outline) as used in the experiments and the locations of the flush-mounted wall probes (Note: at the location of the open symbol the probe did not provide a measurement). The distance between the maximum T_e, recorded by the lower probe during the Trial-A experiments, and the corresponding value from the simulation is 3.7 mm ($z/L_c \approx 0.1$). The light-colored band that was visible around the channel ring after the Trial-A experiments (Fig. 9-middle-right) disappeared in the Trial-B experiments (Fig. 9-right). T_e measurements were not performed in Trial B.*

B. Erosion of the Channel Walls

1. Comparisons of simulation results with CMM and QCM measurements

Profilometry measurements using a CMM also were performed to determine the net rate of material removal and deposition at the channel walls. Henceforth, we follow the convention that negative and positive values depict net deposition and net erosion, respectively. The CMM measurements were made at four different circumferential locations. In ensuing plots these locations are defined by an azimuth angle θ measured clockwise from the r-axis. The resoluti1on capability of the CMM was $\pm$ 1 mm/kh. A QCM mounted near the thruster also was used to measure the back-sputter rate of carbon. These QCM rates were accurate to $\pm$ 0.001 mm/kh. More detailed information about the erosion diagnostics is provided in our companion paper.[16]

Plotted in Fig. 12 are the CMM measurements in the US configuration after the thruster was operated for 27.9 h. Also plotted is the numerical average rate of the four locations for each wall. The measurements illustrate clearly the characteristic length of the erosion zone. At the inner wall this erosion zone traversed approximately the last 10% of the channel length as shown in Fig. 12-left. Also noted in Fig. 12-left are the negative rates measured along the channel for $z/L_c \lesssim 0.875$. Here the erosion rate was so small that carbon and BN deposition allowed for the build-up of layers of these materials onto the surface. The carbon deposition rate was measured by the QCM to be -0.004 mm/kh. Because the original color of the BN wall is white the deposited carbon was clearly visible upon the completion of the experiments. In the last ~10% of the US channel where the CMM measured detectable erosion (Fig. 12-left), the material remained white as seen in the photograph of Fig. 9-left. In subsequent tests with the same chamfered channel geometry as the one used in the MS configuration but with the magnetic field of the US configuration, the white-colored band was visible again, also in the last ~10% of the channel. This is shown in Fig. 9-middle-left in the photograph labeled "US (chamfered)". The presence of this same white band, suggesting net erosion within this region, illustrates the significance of the magnetic field topology relative to the channel geometry in MS configurations. At the outer wall of the US configuration the erosion zone traversed approximately the last 10-15% of L_c as depicted in Fig. 12-right.
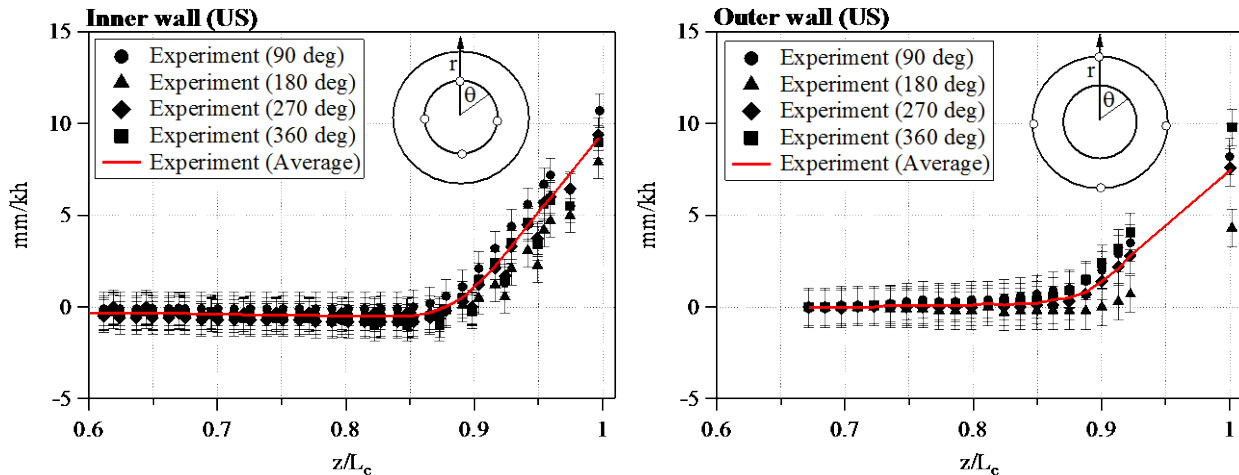

Fig. 12. *Net rate of material removal/deposition measured along the inner (left) and outer (right) channel walls of the US configuration using a CMM. The resolution capability of the CMM was ± 1 mm/kh. The measurements were made at four different circumferential locations defined here by an azimuth angle θ measured clockwise from the r-axis. Also plotted is the numerical average of the four angles. Negative and positive values denote net deposition and net erosion, respectively.*

The erosion rate comparisons between the numerical simulation results and the CMM measurements in US configuration are shown in Fig. 13. It is noted that the simulations did not account for back-sputtered carbon from the facility and re-deposition of BN onto the walls. Also, due to our uncertainty of the sputtering yield at low energies ($\lesssim$ 100 V) results in Fig. 13 are presented for both yield models fI_K

and $f2_K$. As expected the model with higher K_T ($f2_K$) displaces forward (downstream) the location where detectable erosion along the channel begins to occur. Because the two models do not vary significantly at energies $\gtrsim 120$ V, only small differences are observed between the simulation predictions in the last ~5% of the channel. The comparison suggests better correlation between theory and experiment when $f2_K$ is applied. It is possible then that this is a more accurate model of the sputtering yield for this material but, to the best of our knowledge, no direct measurements exist that can confirm this assertion. Also, since the largest discrepancies between simulation and the CMM measurements regarding the location of the erosion zone (~5-8% of L_c) are comparable to our uncertainty of the precise location of the acceleration zone (see discussion in Sec. II.A.2), the possibility that $f1_K$ is ultimately the more accurate model cannot be eliminated. Thus, we present below comparisons using both yield models $f1_K$ and $f2_K$ as discussed in Sec. I.B.1. Finally, it is worthwhile noting that due to the relatively low resolution of the CMM, measured erosion rates that are below 1 mm/kh are ambiguous because they are in the noise of the instrument as illustrated in Fig. 13.
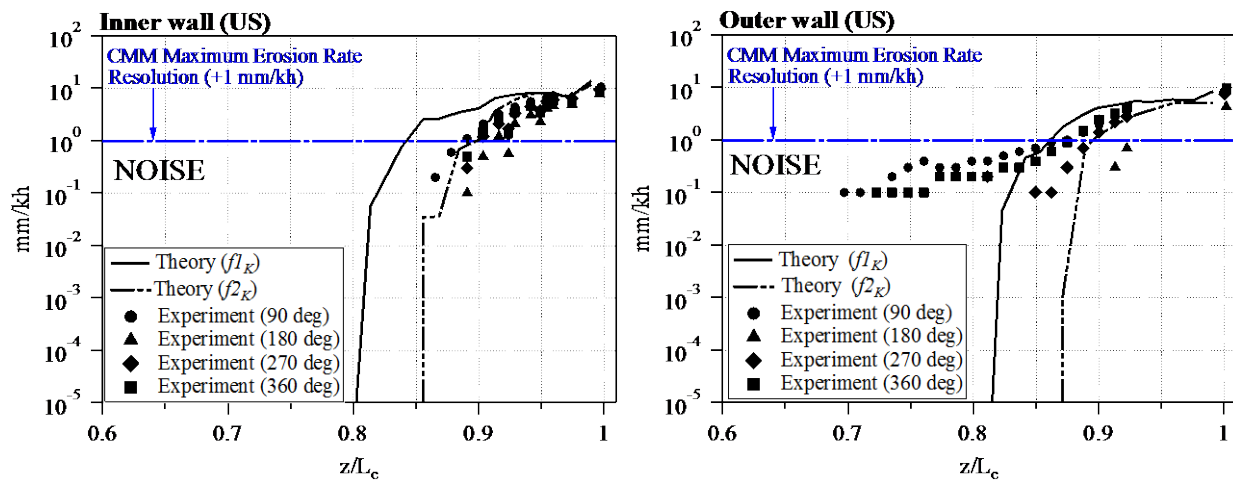

Fig. 13. *Comparisons between simulated and measured erosion rates along the inner (left) and outer (right) channel walls of the US configuration. The two theoretical results correspond to two different sputtering yield models, $f1_K$ ($K_T=25$ V) and $f2_K$ ($K_T=50$ V) as plotted in* Fig. 4. *Notes: (1) deposition of carbon and re-deposition of BN were not accounted for in the numerical simulations and, (2) because the measurements were obtained using a CMM capable of resolving erosion rates $\gtrsim 1$ mm/kh all (positive) recorded values below this limit are in the noise of the instrument.*

The average net rates measured by the CMM are compared with the simulation results for both thruster configurations in Fig. 14. The MS thruster was operated for 19 h. For reasons that will become evident shortly, also depicted on these plots are the CMM noise threshold limits (±1 mm/kh) and the carbon deposition rate measured by the QCM (-0.004 mm/kh). Because the former was significantly higher than the net rates expected in the MS configuration, we have followed the following approach to determine "erosion rates" in the MS configuration.

For the inner MS wall visual inspection of the surfaces after the Trial-A test revealed that ~97% of the wall was heavily coated with carbon while the last ~3% of the wall was only partially discolored by carbon deposits (Fig. 9-middle-right). In the heavily-coated regions the erosion rate was therefore <0.004 mm/kh, which is >1700 times less in the MS configuration than the average erosion rate (6.9 mm/kh) measured in US configuration at $z/L_c=0.97$. Given that the CMM resolution (±1 mm/kh) is >>0.004 mm/kh we have disregarded the profilometry data in these regions of the thruster. In the last 3% of the MS inner wall the maximum CMM measurement still yielded net deposition at an average rate of -0.12 mm/kh. Since this last 3% was only partially-discolored (versus fully-coated with carbon) it may be postulated that the erosion rate in this region was in the range of 0.004-0.12 mm/kh. There is strong

evidence however to support the conclusion that the lower limit (0.004 mm/kh) is closer in order of magnitude to the true erosion rate in this region. First, the upper-limit value (0.12 mm/kh) is also in the noise of the CMM instrument and is therefore ambiguous. Second, when the test was repeated several months later, for about the same thruster operation time (14 h), the partially-discolored region observed in the first test (Trial-A, Fig. 9-middle-right) disappeared; the deposited carbon was clearly seen to coat the whole chamfered region. A photograph of the inner wall after the Trial-B test is contrasted with that of the Trial-A test in Fig. 9-right. And third, using the $f1_K$ sputtering yield model (K_T=25 V), the simulations predict that the erosion was reduced by at least 600 times in this last 3% of the inner wall. Zero erosion was computed when $f2_K$ is used because the ion energies were found to be below K_T (=50 V). Thus, using $\varepsilon_{max} \leq 0.004$ mm/kh for the MS configuration and the (average) measured value for the US configuration, ε_{max}=9.2 mm/kh, then we find that the erosion rate was reduced by $\geq$2300 times at the inner wall.

The comparisons for the outer wall are shown in Fig. 14-right. This wall was observed to be fully coated with carbon upon the conclusion of the MS thruster. The observation is supported by the CMM data in Fig. 14-right which suggest net deposition along the full extent of the chamfered region ($0.72 \lesssim z/L_c \leq 1$). The CMM data that lie in the noise of the instrument are disregarded. Therefore, similar arguments to those made about the inner wall may be made about the erosion reductions. Based on the QCM-derived $\varepsilon_{max} \leq 0.004$ mm/kh for the MS outer wall and the (average) measured value for the US outer wall, ε_{max}=7.5 mm/kh, the erosion was reduced by $\geq$1875 times. The simulations predict that the total energy of ions bombarding this wall was less than the threshold energy when $f1_K$ was used hence zero erosion was computed.
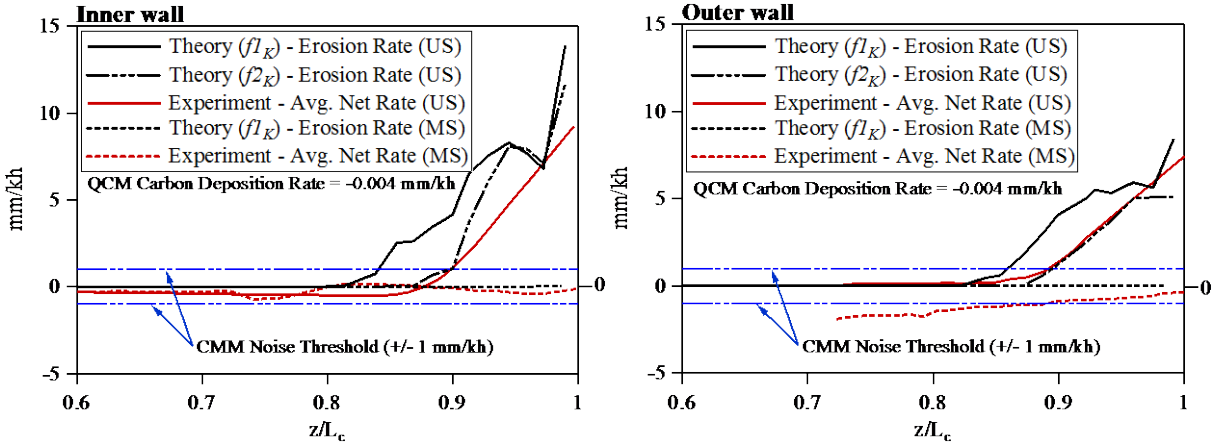

Fig. 14. *Comparisons of the rates of material removal/deposition along inner (left) and outer (right) channel walls in the US and MS configurations. The theoretical results for the US configuration are given for two sputtering yield models $f1_K$ and $f2_K$ (see* Fig. 3-right). *For the MS configuration only $f1_K$ (K_T=25 V) yields a non-zero erosion rate at the inner wall; at the outer wall the computed rate is zero because $K<K_T$. The experimental results are net rates averaged over the four azimuth angles shown in* Fig. 12. *Also plotted are the noise threshold limits of the CMM, ± 1 mm/kh. The carbon deposition rate was measured by a QCM with resolution capability of 0.001 mm/kh. The chamfered walls in the MS configuration span $0.72 \lesssim z/L_c \leq 1$.*

2. Sensitivities

Because some uncertainty exists regarding the precise axial location of the acceleration zone ($\Delta z/L_c \sim$ 5-8%), as discussed in Sec. II.A.2, we conclude this section with results from numerical simulations that aimed at assessing the sensitivity of the erosion rates on the axial position of the plasma. These simulations, performed in addition to the fiducial case shown in Fig. 15-middle (corresponding to the results of Fig. 7-right), varied deliberately the axial position of the collision frequency ν_α which, in turn, displaced the plasma proportionately in the axial direction. For comparison purposes we shall call the

fiducial simulation "Case 0" (Fig. 15-middle). Results from two additional simulations, Cases 1 & 2, are compared in Fig. 15, right and left respectively. In Case 1 (Fig. 15-right) the plasma was displaced *downstream* of the Case-0 solution by $\Delta z/L_c$=0.095 (3.6 mm). In Case 2 (Fig. 15-left) the plasma was displaced *upstream* by $\Delta z/Lc$=0.145 (5.5 mm). In Fig. 16-left we plot the computed total energy of ions striking the MS inner wall for all three cases. Also shown are the two values of K_T prescribed in the two models $f1_K$ and $f2_K$. Figure 16-right compares the computed ε_{max} for the three cases with the corresponding average value measured on the US inner wall.
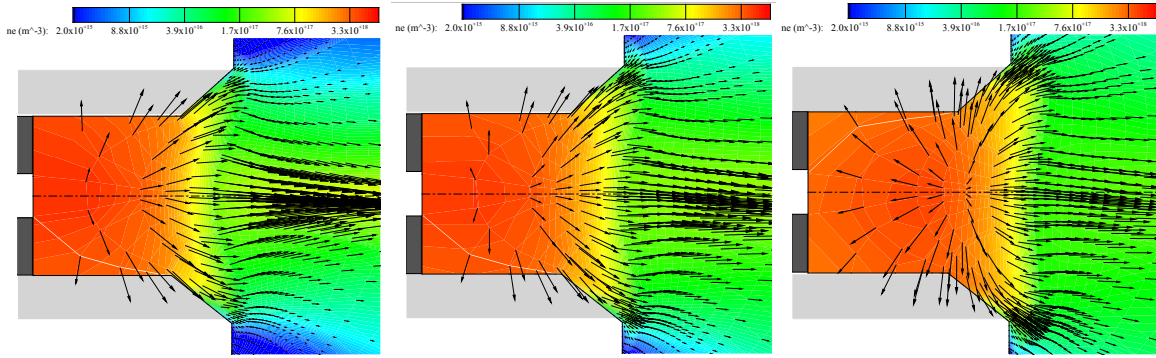

Fig. 15. *Computed electron number density overlaid by flux vectors of Xe+ for three different locations of the acceleration zone in the MS configuration. Case 0 (Middle) is the fiducial case where the location of the plasma is as plotted in* Fig. 7-right*. In Case 1 (right) the plasma in the MS configuration is displaced downstream of the Case-0 solution by $\Delta z/Lc$=0.095 (3.6 mm). In Case 2 (left) the plasma is displaced upstream of the Case-0 solution by $\Delta z/Lc$=0.145 (5.5 mm). The simulations have been performed to assess the sensitivity of the erosion rate in the MS configuration to uncertainties in the location of the interior plasma.*

First, we note in Fig. 16 that both K and ε_{max} increase when the plasma is moved *upstream*, i.e. further into the channel. This occurs despite the reduced ion flux that exists near the chamfered walls. The reason for the increase in ε_{max} is that ε is a strong function of K (through the sputtering yield) at the low energies that are expected to occur along the MS walls, whereas it varies only linearly with the incident ion flux (Eq. (I-5)). Thus, K drives the erosion rate here while the ion flux has a lesser impact. Higher ion energies are obtained in Case 2 because the upstream displacement of the plasma forces a larger variation of the electron number density along the "grazing" lines of force that provide the magnetic shielding of the walls. Thus, a greater $\Delta\phi$ is established along these lines. The opposite arguments may be applied to explain the trends associated with Case 1.

Second, regarding our conclusion in the preceding section on the reductions of the erosion rates in the MS configuration, we find our uncertainty in the location of the acceleration zone to be of little significance. Referring to Fig. 16-right, we note that for Case 1 the ion energy was computed to be below the lowest assumed threshold K_T=25 V; thus, zero erosion was found. For the remaining two simulation cases, using the $f1_K$ model, ε is still found to be >2 orders of magnitude less by comparison to the maximum value measured by the CMM at the US inner wall. This suggests that MS configurations will be insensitive to uncertainties of ~10% in the location of the plasma *if the magnetic field is designed properly*. Indeed, contrary to the small impact that uncertainties in the plasma location may have, accuracy of ≲ 10% in the proximity of magnetic field to the MS walls (e.g. see discussion in Sec.) is critical. This emphasizes the need for a design methodology of MS Hall thrusters that integrates strong participations by numerical simulations and plasma diagnostics.
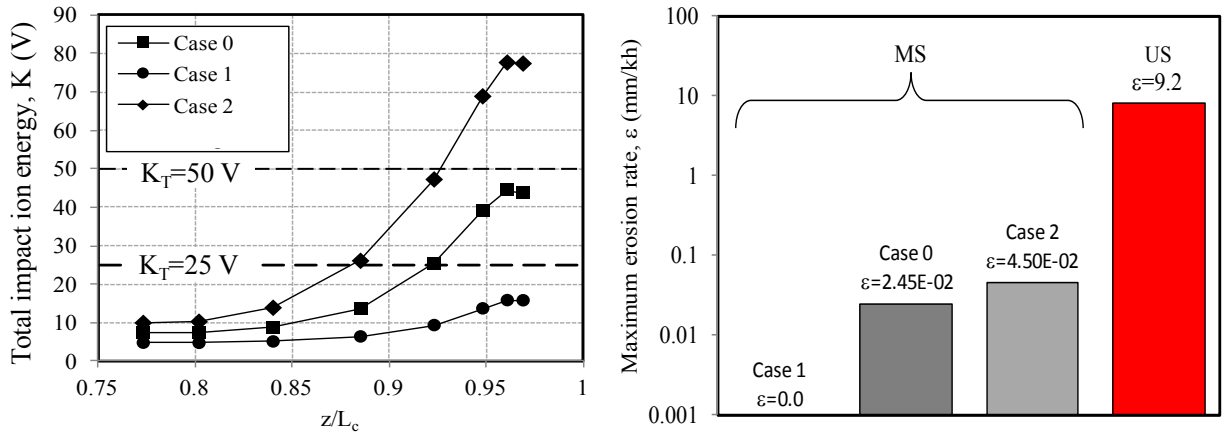
American Institute of Aeronautics and Astronautics

Fig. 16. *Sensitivity of the simulation results in the MS configuration on the axial location of the acceleration region. Left: Total energy of ions striking the MS inner wall. We note that erosion is set to zero in the simulations when $K<K_T$. Right: Maximum erosion rates computed for the three simulation cases at the MS inner wall. Also shown for comparison is the maximum (averaged) erosion rate measured at the inner wall of the US configuration.*

III. Conclusions

In 2009 a proof-of-principle effort began at JPL to demonstrate a technique that takes advantage of specific properties of the lines of force in Hall thruster discharges to eliminate or reduce by orders of magnitude erosion of the acceleration channel. Because magnetic circuit degradation, allowed by channel erosion, constitutes the primary failure mode in these thrusters, if successful, magnetic shielding would extend their throughput to levels that are sufficient for a wide range of new science missions. Such >order-of-magnitude leaps in the life of these thrusters have remained elusive for decades.

Magnetic shielding seeks to achieve ideal equipotentialization of the lines of force near the walls in a manner that reduces significantly the incident energy of ions. The derivation of the first principles of magnetic shielding, and the thruster design that can achieve it, were largely the product of numerical simulations with Hall2De, a physics-based 2-D axisymmetric code that allows for the resolution of the plasma properties at walls near complicated magnetic field topologies. Combined with knowledge about specific properties of the magnetic field lines in these discharges, first deduced by Morozov *et al.* several decades ago, the numerical simulations guided the modifications of an existing laboratory Hall thruster. The MS thruster was built and tested to demonstrate reduced erosion rates. It was recognized and emphasized early in the effort that to achieve reduced erosion rates in the laboratory, albeit necessary, would not be establishing sufficient evidence to complete the demonstration of magnetic shielding. Proof of the physics that led to such reductions would also have to be established. Thruster testing therefore was accompanied by a wide range of plasma and erosion diagnostics to validate the theory.

This is the third and final paper on this 2-yr effort, concluding a series of reports on the design, testing and validation of magnetic shielding in the H6 Hall thruster. In summary, our findings are as follows. Based on the wall-probe measurements, the magnetic field topology relative to the chamfered walls in the MS configuration altered the near wall plasma according to the theoretical predictions. The plasma potential remained at near-V_d values and the electron temperature was at least 2.5-3 times colder than along the US walls. This modification of the plasma properties reduced the impact energy of ions to values that ranged approximately 20-50 V along the MS walls. Comparisons between theory and experiment for the erosion rates in the US configuration suggested that the threshold energy of the BN material used in this thruster is approximately in the same range: 25-50 V. Though, to the best of our knowledge, no direct measurements of the sputtering yield below 50 V exist to confirm this range, we argue that even if the true threshold was in the lower limit erosion would still be considerably lower because the ion flux to the MS walls was also reduced (in addition to the ion energy). QCM and CMM

measurements strongly support these conclusions. Upon termination of the MS thruster tests the walls were visibly coated with carbon for ~97% and 100% of their length in two trials of the same test. Combined with the QCM measurement of the carbon deposition rate (-0.004 mm/kh) we concluded that the erosion rate was reduced by at least three orders of magnitude in the MS configuration. These rates were significantly below the resolution of the CMM instrument (± 1 mm/kh).

The comparisons between theory and experiment identify also areas where better understanding is required. We found differences between the magnetic field produced by a commercial software (and used in all numerical simulations), and that applied in the thruster tests. This is not uncommon but due to the importance of the magnetic field near the walls of the MS configuration, identifying the source(s) of the discrepancy becomes more critical here. Some of these discrepancies in the magnetic field were in fact found to be the likely source of the discrepancy found between the wall-probe plasma measurements and the simulation results in the US configuration. It is possible that this discrepancy in the magnetic field also is the source of the much lower (about 10 times) electron temperatures predicted by the simulation near the walls of the MS configuration. This however cannot be confirmed at present. We plan to extend our preliminary simulations with the measured (instead of the simulated) magnetic field to elucidate these differences. Finally, there remains some uncertainty in the simulations and the experiments regarding the precise location of the acceleration zone. A series of sensitivity simulations however confirmed that these uncertainties are of little significance in configurations with strong magnetic shielding.

Collectively, the comparisons between the numerical simulation results and the measurements provide strong evidence that the first principles of magnetic shielding are now well understood and can be applied to reduce erosion in Hall thrusters by at least a few orders of magnitude. At present, this capability can be claimed only for a single operating condition, but work is already underway to demonstrate magnetic shielding at different power levels and discharge voltages.

Acknowledgments

References

[1] A. I. Morozov, and V. V. Savelyev, "Fundamentals of Stationary Plasma Thruster Theory," *Reviews of Plasma Physics*, 21, 203 (2000).

[2] Morosov, A. I., "Focusing of Cold Quasineutral Beams in Electromagnetic Fields," Soviet Physics - Doklady 10, 8 (1966).

[3] Morosov, A. I., Esipchuk, Y. V., Tilinin, G. N., Trofimov, A. V., Sharov, Y. A., and Shchepkin, G. Y., "Plasma Accelerator with Closed Electron Drift and Extended Acceleration Zone," Soviet Physics Technical Physics 17, 1, 38-45 (1972).

[4] D. Manzella, R. Jankovsky, and R. R. Hofer, "Laboratory Model 50 kW Hall Thruster," AIAA Paper No. 02-3676 (2002).

[5] P. Peterson, D. Manzella, and J. John, "The Performance and Wear Characterization of a High-Power High-Isp NASA Hall Thruster," AIAA Paper No. 05-4243 (2005).

[6] R. R. Hofer, and A. D. Gallimore, "High-Specific Impulse Hall Thrusters, Part 1: Influence of Current Density and Magnetic Field," *J. Propul. Power*, 22, 4, 721-731 (2006).

[7] B. Welander, *et al.*, "Life and Operating Range Extension of the BPT-4000 Qualification Model Hall Thruster," AIAA Paper No. 06-5263 (2006).

[8] H. Kamhawi, D. H. Manzella, L. Pinero, T. Haag, A. Mathers, and H. Liles, "In-Space Propulsion High Voltage Hall Accelerator Development Project Overview," AIAA Paper No. 10-6860 (2010).

[9] I. G. Mikellides, I. Katz, R. R. Hofer, D. M. Goebel, K. de Grys, and A. Mathers, "Magnetic Shielding of the Channel Walls in a Hall Plasma Accelerator," *Phys. Plasmas*, 18, 3, 033501 1-18 (2011).

[10] I. G. Mikellides, I. Katz, R. R. Hofer, and D. M. Goebel, "Hall-Effect Thruster Simulations with 2-D Electron Transport and Hydrodynamic Ions," IEPC Paper No. 09-114 (2009).

[11] Y. Raitses *et al.*, J Appl Phys **92** (2002).

[12] Mikellides, I. G., Katz, I., Hofer, R. R., and Goebel, D. M., "Design of a Laboratory Hall Thruster with Magnetically Sh16ielded Channel Walls, Phase I: Numerical Simulations," AIAA Paper 11-5809, July 2011.

[13] G. Kornfeld, N. Koch, H. Harmann, "Physics and Evolution of HEMP-Thrusters," IEPC Paper No. 07-108 (2007).

[14] D. G. Courtney, P. Lozanoy, and M. Martinez-Sanchez, "Continued Investigation of Diverging Cusped Field Thruster," AIAA Paper No. 08-4631 (2008).

[15] J. M. Haas, R. R. Hofer, D. L. Brown, B. M. Reid, and A. D. Gallimore, "Design of the H6 Hall Thruster for High Thrust/Power Investigation," 54th JANNAF Propulsion Meeting, Denver, CO, May 14-17, 2007.

[16] Hofer, R. R., and Goebel, D. M., Mikellides, I. G., Katz, I., "Design of a Laboratory Hall Thruster with Magnetically Shielded Channel Walls, Phase II: Experiments," AIAA Paper 12-XXXX, July 2012.

[17] H. Kamhawi, T. W. Haag, D. T. Jacobson, and D. H. Manzella, "Performance Evaluation of the NASA-300M 20 kW Hall Effect Thruster," AIAA Paper 11-5521 (2011).

[18] I. Katz, and I. G. Mikellides, "Neutral Gas Free Molecular Flow Algorithm Including Ionization and Walls for Use in Plasma Simulations," *J. Comput. Phys*., 230, 4, 1454-1464 (2011).

[19] N. B. Meezan, W. A. Hargus, and M. A. Cappelli, Physical Review E **63** (2001).

[20] A. Ducrocq, J. C. Adam, A. Héron, and G. Laval, "High-Frequency Electron Drift Instability in the Cross-Field Configuration of Hall Thrusters," *Phys. Plasmas,* 13, 102111 (2006).

[21] A. Lazurenko, T. Dudok de Wit, C. Cavoit, V. Krasnoselskikh, A. Bouchoule, and M. Dudeck, "Determination of the Electron Anomalous Mobility Through Measurements of Turbulent Magnetic Field In Hall Thrusters," *Phys. Plasmas*, 14, 033504 (2007).

[22] C. Boniface, L. Garrigues, G. J. M. Hagelaar, J. P. Boeuf, D. Gawron, and S. Mazouffre, "Anomalous Cross Field Electron Transport in a Hall Effect Thruster," *Appl. Phys. Lett*., 89, 161503 (2006).

[23] G. D. Hobbs, and J. A. Wesson, "Heat Flow Through a Langmuir Sheath in the Presence of Electron Emission," *Plasma Phys.*, 9, 85 (1967).

[24] Hofer, R. R., Mikellides, I. G., Katz, I., and Goebel, D. M., "Wall Sheath and Electron Mobility Modeling in Hybrid-PIC Hall Thruster Simulations," AIAA Paper 07-5267, July 2007.

[25] J. Bohdansky, Nucl Instrum Meth B **2** (1984).

[26] E. J., Pencil, T., Randolph, and D. H. Manzella, "End-of-Life Stationary Plasma Thruster Far-Field Plume Characterization," AIAA Paper No. 96-2709 (1996).

[27] Y. Yamamura, and H. Tawara, "Energy Dependence of Ion-Induced Sputtering Yields from Monatomic Solids at Normal Incidence," *Atomic Data and Nuclear Data Tables*, 62, 149-253 (1996).

[28] Hofer, R. R., Mikellides, I. G., Katz, I., and Goebel, D. M., "BPT-4000 Hall Thruster Discharge Chamber Erosion Model Comparison with Qualification Life Test Data," Presented at the 30th International Electric Propulsion Conference, IEPC-2007-267, Florence, Italy, September 17-20, 2007.

[29] B. Rubin, J. L. Topper, and A. P. Yalin, "Total and Differential Sputter Yields of Boron Nitride Measured by Quartz Crystal Microbalance," *J. Phys. D: Appl. Phys.*, 42, 205205 1-11 (2009).

[30] R. Shastry, "Experimental Characterization of the Near-Wall Region in Hall Thrusters and Its Implications on Performance and Lifetime," Ph.D. Dissertation, Aerospace Engineering, University of Michigan, 2011.

[31] James J. Szabo, Noah Z. Warner, Manuel Martinez-Sanchez, "Instrumentation and Modeling of a High Isp Hall Thruster." 38th AIAA/ASME/SAE/ASEE Joint Propulsion Conference & Exhibit, 7-10 July 2002, Indianapolis, Indiana, AIAA 2002-4248.